A Macroscopic Framework for Modeling Heterogeneous Traffic Flows on Urban Networks

Agatha Joumaa, Paola Goatin, Giovanni De Nunzio

A Macroscopic Framework for Modeling Heterogeneous Traffic Flows on Urban Networks

Agatha Joumaa[1,2], Paola Goatin[1], and Giovanni De Nunzio[2]

[1]Université Côte d'Azur, Inria, CNRS, LJAD, 2004 route des Lucioles - BP 93, 06902 Sophia Antipolis Cedex, France;
[2]IFP Energies nouvelles, Rond-point de l'échangeur de Solaize, BP 3, 69360 Solaize, France

ABSTRACT

This study introduces a flexible macroscopic model for heterogeneous traffic flow on general road networks, allowing the presence of several vehicle classes with general speed functions and different maximal densities pertinent to urban environments. The model, applicable to shared road situations, is designed for describing both creeping phenomena and class-specific lane discipline. Extended to networks, the model addresses the dynamics at general $m \times n$ junctions by prescribing suitable coupling conditions. Using the passenger-car-equivalent representation, numerical experiments demonstrate the model's effectiveness in handling different real-life traffic scenarios, each with their complexities. The study focuses on the assessment of total travel time and CO_2 emissions in the network, highlighting influences from various factors and traffic management strategies such as route guidance and modal shift. Results show that the model can accurately describe scenarios of congested situations where cyclists navigate past queues of cars and cars overtake queues of trucks.

KEYWORDS

Multi-class macroscopic traffic flow models on networks; Hyperbolic systems of conservation laws; Finite volume schemes; Traffic management

1. Introduction

Traffic congestion is a problem that increasingly affects urban road users. In recent times, the multimodal nature of traffic is surprisingly leading to undesired congestion patterns due to the different speeds of the different modes of transport, especially in the absence of dedicated road infrastructure for soft modes or public transport. This problem is expected to worsen over time if the present pattern persists (Jia et al. 2015). Therefore, it is important to develop heterogeneous models able to capture the essential features of mixed traffic flows. These models can then be used to assist in easing the traffic problems commonly found in urban networks.

Since two decades, extensive research has focused on integrating traffic heterogeneity and explaining how different vehicles like cars, trucks, motorcycles, and even autonomous vehicles interact on roads. To this aim, the Lighthill-Whitham-Richards (LWR) model (Lighthill and Whitham 1955, Richards 1956) has been extended to model multi-class flows (Benzoni-Gavage and Colombo 2003, Chiarello and Goatin 2019, Van Lint et al. 2008, Wong and Wong 2002). Several traffic characteristics can

CONTACT Agatha Joumaa Email: agatha.joumaa@ifpen.fr

be addressed in this framework. For instance, in Chanut and Buisson (2003) heterogeneity among vehicles is modeled depending on their length and speed. The model in Zhang and Jin (2002) addresses a mixed flow of cars and trucks based on the free flow speed difference. However, in these models, critical and jam density parameters are the same for all vehicle classes. By allowing more general fundamental diagrams, it is possible to model mixed bicycle-car traffic as in Wierbos et al. (2021), powered two-wheelers and cars as in Gashaw et al. (2018), Nair et al. (2011), and even speed differentials and capacity reduction caused by buses as in Liu et al. (2015).

In this setting, overtaking, that is the maneuver of going past other vehicles on the road, is the most common phenomenon (Benzoni-Gavage and Colombo 2003, Tiaprasert et al. 2017). However, other interaction phenomena are more specific to some vehicle classes, such as creeping of smaller vehicles (e.g. bikes) through the gaps left by larger vehicles at stop. Fan and Work (2015) presented a heterogeneous traffic model with two vehicle classes to describe this situation. Their model captures creeping by using a multi-class cell transmission model in the non-creeping phase and a scalar cell transmission model in the creeping phase. In particular, creeping can also be seen as flow through porous media, see e.g. Gashaw et al. (2018), Nair et al. (2011).

The multi-class model in Fan and Work (2015) integrates a specific maximum density for each vehicle class, and the equilibrium speed is expressed as a function of the total occupied space, yet considering specific linear speed functions that can never intersect for the aim of simplicity and to guarantee the hyperbolicity of the model. The latter is an essential property of a multi-class traffic model. In Zhang et al. (2003), it is still unknown and is just assumed to exist. In Benzoni-Gavage and Colombo (2003), the existence of an entropy function acting as a symmetriser was used to demonstrate hyperbolicity in the case of linear class-specific speed functions; however, the method cannot be extended to more general cases. Zhang et al. (2006) proved hyperbolicity under weaker assumptions, allowing more general, strictly decreasing but possibly intersecting speed functions. Nonetheless, they do not consider non strictly decreasing speed functions in their work, which is important for the use of a triangular fundamental diagram, for example.

Additionally to hyperbolicity, another important property of traffic modeling is anisotropy, which means that traffic flow is influenced by the traffic state in front and not from the back. Logghe and Immers (2008) demonstrate that some of the above models may violate anisotropy, when using speed functions that depend on the total road density rather than class-specific densities. However, the use of a triangular fundamental diagram for slow vehicles would prevent their speed in free flow to be affected by the the presence of faster vehicles. This issue was further discussed by Qian et al. (2017), who focus on pragmatic road space allocation and perceived densities to manage cross-class interactions, and Li et al. (2022), who propose a user-equilibrium framework and a Lagrangian representation to ensure anisotropy, especially for mixed human and autonomous vehicle traffic. While these approaches are insightful, their complexity makes them challenging to analyze and adapt for multi-class systems and networks.

Macroscopic flow models are frequently used to assess the overall traffic performance by analyzing specific metrics. They are usually evaluated under the "passenger car equivalent" (`pce`) criterion, that converts the heterogeneous traffic flow to a hypothetical homogeneous one (Shalini and Kumar 2014). `Pce` is the count of passenger cars that will result in identical operational conditions as a vehicle of a different class (e.g. trucks), under the same traffic and control conditions on the roadway. The concept was first introduced by the Highway Capacity Manual (1965) and the values depend on

the vehicle class and traffic conditions (Praveen and Arasan 2013). It should be chosen based on vehicles' size, speed, headway, as well as other variables (Adnan 2014). Nevertheless, only a limited number of models specify the `pce` value based on the traffic state, see e.g. Van Lint et al. (2008).

In this paper, we consider a macroscopic multi-class traffic flow model, accounting for general class-specific speed functions that depend on the total density of vehicles and can intersect or even (partially) coincide. We then extend the model to general road networks, providing coupling conditions at generic $m \times n$ junctions with class specific distribution coefficients and priorities based on any given Riemann solver, see e.g. Daganzo (1995), Garavello et al. (2016) and Jin (2017). We remark that previous works on multi-class flows on networks (Herty et al. 2006, Li and Li 2017, Tuerprasert and Aswakul 2010, Van Lint et al. 2008) were restricted to few classes and specific junction conditions.

For simulation purposes, we show the well-posedness of an adapted Godunov scheme (Godunov 1959) using the corresponding supply-demand formulation (Lebacque 1996). This allows us to run experiments on a network of thirteen roads, showing the interaction among three classes of vehicles that are characterized by their different free-flow speeds and maximal densities. The model allows to capture the dynamics of traffic scenarios commonly encountered on urban roads: it can account for different lane discipline, creeping effects, and describe complex interactions between vehicles of different types. For each considered scenario, we compute two traffic metrics (total travel time and CO_2 emission) to shed light on the advantages of different traffic policies.

To summarize, the main contributions of this work are the following:

- We consider a macroscopic model for traffic flow involving any number of different vehicle classes characterized by the respective mean speed functions, which are assumed to be general non-increasing functions depending solely on the total density of the road, eventually crossing each-other or even locally coinciding. This flexibility addresses the complexities of real word traffic scenarios, providing a more accurate representation of heterogeneous traffic dynamics. In particular, the model can capture class-specific lane discipline and creeping effects.
  We provide a general proof of the hyperbolicity of the model, thus extending the result in Zhang et al. (2006), and the well-posedness of the associated Godunov scheme, deriving precise stability conditions.
- We propose an extension to road networks, providing coupling conditions at generic $m \times n$ junctions based on the notion of Riemann solver.
- Using the `pce` concept, we apply the model to evaluate different traffic metrics like the total travel time (TTT) and the total CO_2 emissions (TE_{CO2}) under different realistic traffic policies. We present a numerical study involving three distinct types of vehicles, in which we explore the proposed model's sensitivity to two application scenarios: lane restriction and modal shift. This demonstrates the versatility and robustness of the proposed approach.

The rest of the paper is organized as follows. In Section 2, we present the model and prove its hyperbolicity along with the well-posedness of the numerical scheme. Section 3 extends the model to networks addressing the multi-class dynamics to generic junctions. We also describe the treatment of inflow and outflow boundary conditions at origin and destination nodes of the network. In Section 4, we provide numerical results for a sample network, where we compute the TTT and TE_{CO2} depending on different parameter choices. Finally, we conclude the paper in Section 5, where we

discuss future work.

2. Multi-class Traffic Model with General Speed Function

Following Benzoni-Gavage and Colombo (2003), Fan and Work (2015), Garavello et al. (2010), we consider the $M \times M$ system of conservation laws

$$\boldsymbol{\rho}_t + \mathbf{F}(\boldsymbol{\rho})_x = 0, \tag{1}$$

where

$$\boldsymbol{\rho} = (\rho^1, \dots, \rho^M)^T, \quad \mathbf{F}(\boldsymbol{\rho}) = (v^1(r)\rho^1, \dots, v^M(r)\rho^M)^T, \text{ and } r = \sum_{c=1}^{M} \rho^c \tag{2}$$

are respectively the density, the flux function, and the total density. We assume

$$\frac{\mathrm{d}v^c}{\mathrm{d}r}(r) \leq 0, \tag{3}$$

where $v^c(r)$ is the class specific speed s.t.

$$v^c(0) = V^c, \quad \exists R^c \text{ s.t. } v^c(r) = 0 \text{ for } r \geq R^c \tag{4}$$

for $c = 1, \dots, M$ and R^c is the class specific maximal density. Without loss of generality, we also assume that the free flow speeds satisfy

$$V^1 \geq \dots \geq V^M, \tag{5}$$

while we do not require any ordering of $\{R^c\}_{c=1}^M$, see Figure 1.

System (1) is then defined on the convex set:

$$\mathcal{S} = \left\{ \boldsymbol{\rho} \in \mathbb{R}^M : 0 \leq \rho^c \leq R^c \text{ and } \sum_{c=1}^{M} \rho^c \leq R \right\},$$

where $R := \max\{R^1, \dots, R^M\}$.

2.1. Hyperbolicity

In the following, we generalize the result of Zhang et al. (2006), which was restricted to strictly decreasing speed functions, to prove the hyperbolicity of model (1)-(4).

Theorem 2.1. *Under hypotheses* (3) *and* (4)*, the Jacobian of* $\mathbf{F}$ *has* M *bounded real eigenvalues; thus system* (1) *is hyperbolic on* $\mathcal{S}$*.*

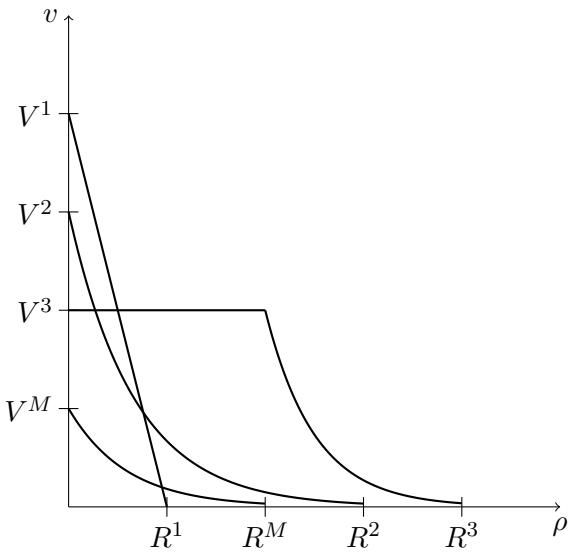

Figure 1.: Example of family of speed functions v^c, $c = 1, \dots, M$, considered in this work

Proof. The jacobian of $\mathbf{F}(\boldsymbol{\rho})$ writes:

$$D\mathbf{F}(\boldsymbol{\rho}) = \begin{pmatrix} v^1+u^1 & u^1 & \dots & u^1 & u^1 \\ u^2 & v^2+u^2 & \dots & u^2 & u^2 \\ \dots & \dots & \dots & \dots & \dots \\ u^{M-1} & u^{M-1} & \dots & v^{M-1}+u^{M-1} & u^{M-1} \\ u^M & u^M & \dots & u^M & v^M+u^M \end{pmatrix}, \qquad u^c = \rho^c \frac{\mathrm{d}v^c}{\mathrm{d}r} \leq 0. \tag{6}$$

Here, we note that $u^c = 0$ if and only if $\rho^c = 0$ or $\frac{\mathrm{d}v^c}{\mathrm{d}r}(r) = 0$. We rewrite

$$\begin{aligned} P_M(\lambda) &:= \det(D\mathbf{F}(\boldsymbol{\rho}) - \lambda I) \\ &= \begin{vmatrix} v^1+u^1-\lambda & u^1 & \dots & u^1 & u^1 \\ u^2 & v^2+u^2-\lambda & \dots & u^2 & u^2 \\ \dots & \dots & \dots & \dots & \dots \\ u^{M-1} & u^{M-1} & \dots & v^{M-1}+u^{M-1}-\lambda & u^{M-1} \\ u^M & u^M & \dots & u^M & v^M+u^M-\lambda \end{vmatrix} \end{aligned} \tag{7}$$

taking $(v^c - \lambda)$ out as a factor from the *c-th* row, $c = 1, \dots, M$, so that (7) has the form

$$P_M(\lambda) = \prod_{c=1}^{M}(v^c-\lambda) \begin{vmatrix} 1+K_1 & K_1 & \dots & K_1 & K_1 \\ K_2 & 1+K_2 & \dots & K_2 & K_2 \\ \dots & \dots & \dots & \dots & \dots \\ K_{M-1} & K_{M-1} & \dots & 1+K_{M-1} & K_{M-1} \\ K_M & K_M & \dots & K_M & 1+K_M \end{vmatrix}, \qquad K_c = \frac{u^c}{v^c-\lambda}\,. \tag{8}$$

Then we add the first $(M-1)$ rows to the last row, so that all its elements are identical

and we have

$$P_M(\lambda) = \prod_{c=1}^{M}(v^c - \lambda)Q_M(\lambda), \qquad Q_M(\lambda) = 1 + \sum_{c=1}^{M} K_c(\lambda)\,, \tag{9}$$

since

$$\begin{vmatrix} 1+K_1 & K_1 & \dots & K_1 & K_1 \\ K_2 & 1+K_2 & \dots & K_2 & K_2 \\ \dots & \dots & \dots & \dots & \dots \\ K_{M-1} & K_{M-1} & \dots & 1+K_{M-1} & K_{M-1} \\ 1 & 1 & \dots & 1 & 1 \end{vmatrix} = \det(I) = 1\,.$$

We distinguish different cases:

Case 1: $u^c < 0,\ \forall c$ and

$$v^{\sigma(1)}(r) < v^{\sigma(2)}(r) < \ldots < v^{\sigma(M-1)}(r) < v^{\sigma(M)}(r), \tag{10}$$

for some permutation $\sigma \in S_M$. We can verify that by (9)-(10), we have

$$\operatorname{sgn}\left(P_M(v^c)\right) = (-1)^{\sigma(c)},\ c = 1, \ldots, M; \qquad \operatorname{sgn}\left(P_M(v^{\sigma(1)} + \sum_{c=1}^{M} u^c)\right) = 1 \tag{11}$$

by evaluating $P_M(\lambda)$ at $\lambda = v^c$ as follows. We first observe that the product $\prod_{c=1}^{M}(v^c - \lambda)$ changes sign depending on the number of negative factors, so using (10), we consider the intervals defined by the ordered $v^{\sigma(c)}(r)$:

- for $\lambda < v^{\sigma(1)}(r)$: all $v^c - \lambda > 0$, so the product $\prod_{c=1}^{M}(v^c - \lambda) > 0$, each $K_c(\lambda)$ is finite and negative (since $u^c < 0$ and $v^c - \lambda > 0$) and $Q_M(\lambda) = 1 + \sum_{c=1}^{M} K_c(\lambda)$ is less than 1 but positive, therefore, $\operatorname{sgn}(P_M(\lambda)) = +1$.
- for $v^{\sigma(c-1)}(r) < \lambda < v^{\sigma(c)}(r)$ (with $c \geq 2$), we have $c-1$ negative terms $(v^{\sigma(i)} - \lambda)$ (for $i = 1, \ldots, c-1$) and $M - (c-1)$ positive terms, so the product $\prod_{c=1}^{M}(v^c - \lambda)$ has sign $(-1)^{c-1}$, while $K_{\sigma(c-1)}(\lambda) > 0$, so $Q_M(\lambda)$ is positive. Therefore, $\operatorname{sgn}(P_M(\lambda)) = (-1)^{c-1}$.
- for $\lambda > v^{\sigma(M)}(r)$, all $v^c - \lambda < 0$, so $\prod_{c=1}^{M}(v^c - \lambda) > 0$ if M is even, and < 0 if M is odd, each $K_c(\lambda)$ is finite and positive so $Q_M(\lambda) = 1 + \sum_{c=1}^{M} K_c(\lambda) > 1$, therefore, $\operatorname{sgn}(P_M(\lambda)) = (-1)^M$.

Finally, for $\lambda = v^c$, $\operatorname{sgn}\left(P_M(v^c)\right) = (-1)^{\sigma(c)},\ c = 1, \ldots, N$;
As for $\operatorname{sgn}\left(P_M(v^{\sigma(1)} + \sum_{c=1}^{M} u^c)\right)$, since $u^c < 0,\ \forall\ c$, then $\sum_{c=1}^{M} u^c < 0$ then $v^{\sigma(1)} + \sum_{c=1}^{M} u^c < v^{\sigma(1)}$, so we are back at the first discussed point when $\lambda < v^{\sigma(1)}$, and the sign is positive.

By the intermediate value theorem, (11) implies that the polynomial $P_M(\lambda)$ has M

real distinct bounded roots $\{\lambda^c\}_{c=1}^M$ such that

$$v^{\sigma(1)} + \sum_{c=1}^{M} u^c < \lambda^1 < v^{\sigma(1)}(r) < \lambda^2 < v^{\sigma(2)}(r) < \ldots < v^{\sigma(c-1)}(r) < \lambda^c < v^{\sigma(c)}(r) < \ldots \\ \ldots < v^{\sigma(M-1)}(r) < \lambda^M < v^{\sigma(M)}(r). \tag{12}$$

In this case, the system is strictly hyperbolic.

Case 2: At least two $v^c(r)$ are equal or at least one u^c is zero ($\rho^c = 0$ or $\frac{\mathrm{d}v^c}{\mathrm{d}r}(r) = 0$). We proceed by induction on M. The conclusion is obvious for $M = 1$, because the Jacobian matrix $D\mathbf{F}(\rho)$ is scalar. Assuming that this is true for all l, $l = 1, \ldots, M-1$, we prove it is also true for $l = M$. By (9), this case is equivalent to having an eigenvalue $\lambda = v^c(r)$ of multiplicity at least 2. We can always find another permutation $\tau \in S_M$ such that $\lambda = v^{\tau(M-k)}(r) = \ldots = v^{\tau(M)}(r)$, for some $0 \leq k < M$. Here, $v^{\tau(M)}(r)$ is not equal to any other $v^c(r)$, and $\{v^{\tau(c)}(r)\}_{c=1}^M$ do not necessarily follow the sequence of (10). In this case, (9) can be rewritten as

$$P_M(\lambda) = (v^{\tau(M)}(r) - \lambda)^k \tilde{P}_{M-k}(\lambda), \tag{13}$$

where

$$\tilde{P}_{M-k}(\lambda) = \prod_{c=1}^{M-k} (v^{\tau(c)}(r) - \lambda)\tilde{Q}_{M-k}(\lambda), \quad \tilde{Q}_{M-k}(\lambda) = 1 + \sum_{c=1}^{M-k} \tilde{K}_{\tau(c)}.$$

and

$$\tilde{K}_{\tau(c)} = K_{\tau(c)} \text{ for } c \leq M-k-1, \qquad \tilde{K}_{\tau(M-k)} = \frac{\tilde{c}_{\tau(M-k)}}{v^{\tau(M-k)} - \lambda}, \ \tilde{c}_{\tau(M-k)} = \sum_{i=N-k}^{M} u^{\tau(i)} \leq 0$$

For $k \geq 1$, all roots of $P_M(\lambda)$ are real, simply by (12) or the assumption for l on the polynomial $\tilde{P}_{M-k}(\lambda)$ of (13), since by the induction hypothesis we assumed that $\tilde{P}_l(\lambda)$ has l real roots for $l \in \{1, \ldots, M-1\}$, so $\tilde{P}_{M-k}(\lambda)$ has $M-k$ real roots.
For $k = 0$, $\lambda = v^{\tau(M)}(r)$ being an eigenvalue is equivalent to have $u^{\tau(M)} = 0$. This means that

$$P_M(\lambda) = (v^{\tau(M)}(r) - \lambda)P_{M-1}(\lambda),$$

So $P_M(\lambda)$ has M real roots. In both cases, the system is hyperbolic. □

From the above proof, it is straightforward to conclude the following.

Corollary 2.2. *$v^j(r) \in \{v^c(r)\}_{c=1}^M$ is an eigenvalue of the Jacobian matrix $D\mathbf{F}(\boldsymbol{\rho})$ if and only if $\rho^c = 0$ or $\frac{\mathrm{d}v^c}{\mathrm{d}r}(r) = 0$ or $\exists\ l \neq c$, s.t. $v^l(r) = v^c(r)$.*

Corollary 2.3. *If the characteristic polynomial $P_M(\lambda)$ of the Jacobian matrix $D\mathbf{F}(\boldsymbol{\rho})$ has a multiple root λ, then $\lambda \in \{v^c(r)\}_{c=1}^M$.*

2.2. *Finite volume discretization*

Following Bürger et al. (2008) and Briani and Cristiani (2014), we approximate system (1) by the Godunov finite volume scheme Godunov (1959) in its supply/demand formulation Lebacque (1996):

$$\rho_j^{c,\nu+1} = \rho_j^{c,\nu} - \frac{\Delta t}{\Delta x}\left[F_{j+1/2}^{c,\nu} - F_{j-1/2}^{c,\nu}\right], \qquad j \in \mathbb{Z},\ \nu \in \mathbb{N},\ c = 1, \dots, M, \tag{14}$$

where ν is the time step index, j the spatial index, Δx and Δt are the space and time meshes and

$$F_{j+1/2}^{c,\nu} := \frac{\rho_j^{c,\nu}}{r_j^\nu} \min\left\{D^c(r_j^\nu), S^c(r_{j+1}^\nu)\right\}, \tag{15}$$

with D^c and S^c respectively the demand and supply functions of the total density relatively to the c-th class speed, which are defined by setting $Q^c(r) := rv^c(r)$, $r_{cr}^c := \arg\max_r Q^c(r)$ and

$$D^c(r) := Q^c(\min\{r, r_{cr}^c\}), \tag{16}$$
$$S^c(r) := Q^c(\max\{r, r_{cr}^c\}). \tag{17}$$

See also (Levin and Boyles 2016, Eq. (4)).

In the following, we provide a refined Courant-Friedrichs-Lewy (CFL) stability condition (Courant et al. 1928) for the numerical scheme (14)-(17), ensuring the positivity and boundedness of approximate solutions.

Proposition 2.4. *Under the CFL condition*

$$\max\left\{\max_c \|v^c\|_\infty, \max_c \left\|\frac{\mathrm{d}Q^c}{\mathrm{d}r}\right\|_\infty\right\} \Delta t \le \Delta x\,, \tag{18}$$

for any initial data $\boldsymbol{\rho}_0 \in \mathcal{S}$ the approximate solutions computed by the Godunov scheme (14) - (17)*, satisfy the following uniform bounds:*

$$\boldsymbol{\rho}_j^\nu \in \mathcal{S} \quad \forall j \in \mathbb{Z},\ \nu \in \mathbb{N}.$$

Proof. We proceed by induction: assuming that $\rho_j^{c,\nu} \in [0, R^c]$ for $c = 1, \dots, M$, and $\sum_{c=1}^M \rho_j^{c,\nu} \le R$ for all $j \in \mathbb{Z}$, we show that the same holds for $\boldsymbol{\rho}_j^{\nu+1}$. In the following, we drop the index ν.

Regarding positivity,

$$\begin{aligned}
\rho_j^{c,\nu+1} &= \rho_j^c - \frac{\Delta t}{\Delta x}\left[F^c_{j+\frac{1}{2}} - F^c_{j-\frac{1}{2}}\right] \\
&= \rho_j^c - \frac{\Delta t}{\Delta x}\left[\frac{\rho_j^c}{r_j}\min\left\{D^c(r_j), S^c(r_{j+1})\right\} - \frac{\rho_{j-1}^c}{r_{j-1}}\min\left\{D^c(r_{j-1}), S^c(r_j)\right\}\right] \\
&\geq \rho_j^c - \frac{\Delta t}{\Delta x}\frac{\rho_j^c}{r_j}\min\left\{D^c(r_j), S^c(r_{j+1})\right\} \\
&\geq \rho_j^c - \frac{\Delta t}{\Delta x}\frac{\rho_j^c}{r_j}D^c(r_j) \\
&= \rho_j^c - \frac{\Delta t}{\Delta x}\frac{\rho_j^c}{r_j}Q^c(\min\{r_j, r^c_{cr}\}) \\
&= \rho_j^c - \frac{\Delta t}{\Delta x}\frac{\rho_j^c}{r_j}\min\{r_j, r^c_{cr}\}v^c(\min\{r_j, r^c_{cr}\}) \\
&\geq \rho_j^c - \frac{\Delta t}{\Delta x}\frac{\rho_j^c}{r_j}r_j v^c(\min\{r_j, r^c_{cr}\}) \\
&= \rho_j^c\left(1 - \frac{\Delta t}{\Delta x}v^c(\min\{r_j, r^c_{cr}\})\right) \geq 0
\end{aligned}$$

if $\Delta t\|v^c\|_\infty \leq \Delta x$.

On the other side,

$$\begin{aligned}
\rho_j^{c,\nu+1} &= \rho_j^c - \frac{\Delta t}{\Delta x}\left[F^c_{j+\frac{1}{2}} - F^c_{j-\frac{1}{2}}\right] \\
&= \rho_j^c - \frac{\Delta t}{\Delta x}\left[\frac{\rho_j^c}{r_j}\min\left\{D^c(r_j), S^c(r_{j+1})\right\} - \frac{\rho_{j-1}^c}{r_{j-1}}\min\left\{D^c(r_{j-1}), S^c(r_j)\right\}\right] \\
&\leq \rho_j^c + \frac{\Delta t}{\Delta x}\frac{\rho_{j-1}^c}{r_{j-1}}\min\left\{D^c(r_{j-1}), S^c(r_j)\right\} \\
&\leq \rho_j^c + \frac{\Delta t}{\Delta x}\frac{\rho_{j-1}^c}{r_{j-1}}S^c(r_j)\,.
\end{aligned}$$

Setting

$$\phi(\rho^c) := \rho^c + \frac{\Delta t}{\Delta x}\frac{\rho^c_{j-1}}{r_{j-1}}S^c(r),$$

we get $\phi(R^c) = R_c$ and

$$\frac{\mathrm{d}\phi}{\mathrm{d}\rho^c}(\rho^c) = 1 + \frac{\Delta t}{\Delta x}\frac{\rho^c_{j-1}}{r_{j-1}}\frac{\mathrm{d}S^c}{\mathrm{d}r}(r) \geq 1 - \frac{\Delta t}{\Delta x}\frac{\rho^c_{j-1}}{r_{j-1}}\left\|\frac{\mathrm{d}S^c}{\mathrm{d}r}\right\|_\infty \geq 1 - \frac{\Delta t}{\Delta x}\left\|\frac{\mathrm{d}S^c}{\mathrm{d}r}\right\|_\infty \geq 0$$

if $\Delta t\left\|\frac{\mathrm{d}Q^c}{\mathrm{d}r}\right\|_\infty \leq \Delta x$. Hence $\phi(\rho^c) \leq R_c$.

Finally,

$$\begin{aligned}\sum_{c=1}^{M}\rho_j^{c,\nu+1} &= \sum_{c=1}^{M}\rho_j^c - \frac{\Delta t}{\Delta x}\sum_{c=1}^{M}\left[F^c_{j+\frac{1}{2}} - F^c_{j-\frac{1}{2}}\right]\\ &= \sum_{c=1}^{M}\rho_j^c - \frac{\Delta t}{\Delta x}\sum_{c=1}^{M}\left[\frac{\rho_j^c}{r_j}\min\left\{D^c(r_j), S^c(r_{j+1})\right\} - \frac{\rho_{j-1}^c}{r_{j-1}}\min\left\{D^c(r_{j-1}), S^c(r_j)\right\}\right]\\ &\le \sum_{c=1}^{M}\rho_j^c + \frac{\Delta t}{\Delta x}\sum_{c=1}^{M}\frac{\rho_{j-1}^c}{r_{j-1}}\min\left\{D^c(r_{j-1}), S^c(r_j)\right\}\\ &\le \sum_{c=1}^{M}\rho_j^c + \frac{\Delta t}{\Delta x}\sum_{c=1}^{M}\frac{\rho_{j-1}^c}{r_{j-1}}S^c(r_j).\end{aligned}$$

Setting

$$\phi(\boldsymbol{\rho}) := \sum_{c=1}^{M}\rho^c + \frac{\Delta t}{\Delta x}\sum_{c=1}^{M}\frac{\rho_{j-1}^c}{r_{j-1}}S^c(r),$$

we get $\phi(\boldsymbol{\rho}) = R$ if $\sum_{c=1}^{M}\rho_j^c = R$ and

$$\begin{aligned}\frac{\partial\phi}{\partial\rho^d}(\boldsymbol{\rho}) &= 1 + \frac{\Delta t}{\Delta x}\sum_{c=1}^{M}\frac{\rho_{j-1}^c}{r_{j-1}}\frac{\partial S^c(r)}{\partial\rho^d}\\ &\ge 1 - \frac{\Delta t}{\Delta x}\sum_{c=1}^{M}\frac{\rho_{j-1}^c}{r_{j-1}}\left\|\frac{\mathrm{d}S^c}{\mathrm{d}r}\right\|_\infty\\ &\ge 1 - \max_c\left\|\frac{\mathrm{d}S^c}{\mathrm{d}r}\right\|_\infty\frac{\Delta t}{\Delta x}\sum_{c=1}^{M}\frac{\rho_{j-1}^c}{r_{j-1}}.\end{aligned}$$

If $\Delta t\max_c\left\|\frac{\mathrm{d}Q^c}{\mathrm{d}r}\right\|_\infty \le \Delta x$, then $1 - \frac{\Delta t}{\Delta x}\max_c\left\|\frac{\mathrm{d}S^c}{\mathrm{d}r}\right\|_\infty \ge 0$ and hence $\phi(\boldsymbol{\rho}) \le R$ for all $\boldsymbol{\rho}\in\mathcal{S}$, where we used that $\sum_{c=1}^{M}\frac{\rho_{j-1}^c}{r_{j-1}} = 1$. □

3. Network Modeling

We consider graphs of directed arcs connected at nodes as a representation of road networks. The main component of the network extension is modeling traffic dynamics at junctions (Daganzo 1995, Garavello et al. 2016). In particular, junction dynamics can be formulated as an optimization problem constrained by the demands of incoming links and the supplies of outgoing roads.

3.1. Junction solver for M classes of vehicles

In the following, we first provide the numerical fluxes for general $m \times n$ junctions (m incoming and n outgoing roads) when M classes of vehicles are involved, and then detail the formulations for simple 1×1 junctions, general $m \times 1$ merges and general

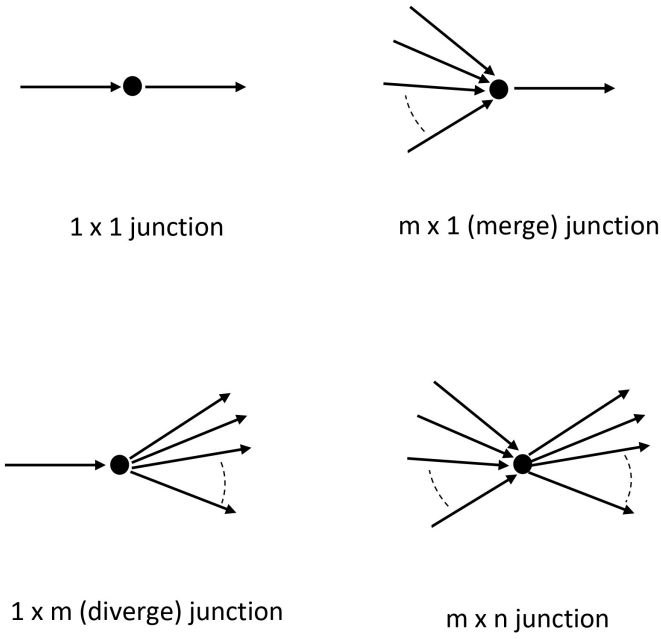

Figure 2.: Types of junctions considered in this work

$1 \times m$ diverges, see Figure 2. Note that, in general, the demand and supply functions given by equations (16) and (17) will be link-specific. Therefore, for any given junction, let us denote by $\mathcal{I}$ the set of incoming roads $i \in \mathcal{I}$, and by $\mathcal{J}$ the set of outgoing roads $j \in \mathcal{J}$. The type of junction is therefore generally defined by the cardinality of the two sets, denoted as $|\mathcal{I}|$ and $|\mathcal{J}|$, respectively.

3.1.1. Solver for general $m \times n$ junction.

Let $|\mathcal{I}| = m$ and $|\mathcal{J}| = n$. We denote by $P^c = (p_i^c)_{i\in\mathcal{I}} \in \mathbb{R}^m$, $p_i^c \geq 0$, $\sum_{i\in\mathcal{I}} p_i^c = 1$ the class specific priority vectors and by A^c the class specific distribution matrices

$$A^c = \left\{ \{a_{ji}^c\} \in \mathbb{R}^{n\times m},\ 0 \leq a_{ji}^c \leq 1,\ \sum_{j\in\mathcal{J}} a_{ji}^c = 1 \right\}$$

where a_{ji}^c indicates the percentage of vehicles of class c going from road i to road j. Using a selected Riemann solver (see e.g. Coclite et al. (2005), Delle Monache et al. (2016), Garavello and Piccoli (2005)), we compute the class specific total fluxes $(\bar{\gamma}_i^c)_{i\in\mathcal{I}}$ corresponding to $D_i^c(r_{i,N_i})$, $i \in \mathcal{I}$, and $S_j^c(r_{j,1})$, $j \in \mathcal{J}$, with A^c and P^c as distribution matrix and priority vector respectively.
We then rescale the fluxes according to the class ratio, so the incoming and outgoing fluxes for each class are given by:

$$\hat{\gamma}_i^c = \frac{\rho_{i,N_i}^c}{r_{i,N_i}} \bar{\gamma}_i^c \quad i \in \mathcal{I}, \qquad \hat{\gamma}_j^c = \sum_{i=1}^{m} a_{ji}^c \hat{\gamma}_i^c, \quad j \in \mathcal{J}. \tag{19}$$

Proposition 3.1. *Under the CFL condition* (18)*, the incoming and outgoing fluxes defined by* (19) *satisfy mass conservation and the incoming fluxes guarantee the invariance of the domain $\mathcal{S}$. Additionally, under the stronger CFL condition*

$$\max\left\{\max_c \|v^c\|_\infty, M\max_c \left\|\frac{\mathrm{d}Q^c}{\mathrm{d}r}\right\|_\infty\right\}\Delta t \le \Delta x\,, \tag{20}$$

the outgoing fluxes ensure the invariance of the domain $\mathcal{S}$.

Proof. Concerning mass conservation, we observe that, for each class c, the total outflow onto the n outgoing roads is:

$$\sum_{j=1}^{n}\hat{\gamma}_j^c = \sum_{j=1}^{n}\sum_{i=1}^{m} a_{ji}^c\hat{\gamma}_i^c = \sum_{i=1}^{m}\hat{\gamma}_i^c\sum_{j=1}^{n} a_{ji}^c = \sum_{i=1}^{m}\hat{\gamma}_i^c,$$

where $\sum_{i=1}^m \hat{\gamma}_i^c$ is the total inflow from the m incoming roads. Summing over all classes $c = 1,\dots,M$ we get:

$$\sum_{c=1}^{M}\sum_{j=1}^{n}\hat{\gamma}_j^c = \sum_{c=1}^{M}\sum_{i=1}^{m}\hat{\gamma}_i^c$$

which confirms total mass conservation at the junction.
To check the invariance of $\mathcal{S}$, we proceed by induction, assuming that at the last cell N_i of any incoming road $i\in\mathcal{I}$, $\rho_{i,N_i}^{c,\nu} \in [0, R_i^c]$ for $c = 1,\dots,M$ and $\sum_{c=1}^M \rho_{i,N_i}^{c,\nu} \le R_i$, we show that the same holds for $\rho_{i,N_i}^{c,\nu+1}$.
In the following, we drop the index ν. Regarding positivity, we get

$$\begin{aligned}
\rho_{i,N_i}^{c,\nu+1} &= \rho_{i,N_i}^c - \frac{\Delta t}{\Delta x}\left[\hat{\gamma}_i^c - F_{i,N_i-\frac{1}{2}}^c\right]\\
&\ge \rho_{i,N_i}^c - \frac{\Delta t}{\Delta x}\hat{\gamma}_i^c\\
&= \rho_{i,N_i}^c - \frac{\Delta t}{\Delta x}\frac{\rho_{i,N_i}^c}{r_{i,N_i}}\bar{\gamma}_i^c\\
&\ge \rho_{i,N_i}^c - \frac{\Delta t}{\Delta x}\frac{\rho_{i,N_i}^c}{r_{i,N_i}}D_i^c(r_{i,N_i})\\
&= \rho_{i,N_i}^c - \frac{\Delta t}{\Delta x}\frac{\rho_{i,N_i}^c}{r_{i,N_i}}\min\{r_{i,N_i}, r_{i,cr}^c\}v_i^c(\min\{r_{i,N_i}, r_{i,cr}^c\})\\
&\ge \rho_{i,N_i}^c - \frac{\Delta t}{\Delta x}\frac{\rho_{i,N_i}^c}{r_{i,N_i}}r_{i,N_i}v_i^c(\min\{r_{i,N_i}, r_{i,cr}^c\})\\
&= \rho_{i,N_i}^c\left(1 - \frac{\Delta t}{\Delta x}v_i^c(\min\{r_{i,N_i}, r_{i,cr}^c\})\right) \ge 0
\end{aligned}$$

where we used the CFL condition (18).
To prove that $\rho_{i,N_i}^c \le R_i^c$ and that $\sum_{c=1}^M \rho_{i,N_i}^c \le R_i$, the proof follows from the proof

of Lemma 2.4.

$$\begin{aligned}
\rho_{i,N_i}^{c,\nu+1} &= \rho_{i,N_i}^{c} - \frac{\Delta t}{\Delta x}\left[\hat{\gamma}_i^c - F_{i,N_i-\frac{1}{2}}^{c}\right] \\
&\leq \rho_{i,N_i}^{c} + \frac{\Delta t}{\Delta x} F_{i,N_i-\frac{1}{2}}^{c} \\
&= \rho_{i,N_i}^{c} + \frac{\Delta t}{\Delta x}\frac{\rho_{i,N_i-1}^{c}}{r_{i,N_i-1}} \min\left\{D_i^c(r_{i,N_i-1}), S_i^c(r_{i,N_i})\right\} \\
&\leq \rho_{i,N_i}^{c} + \frac{\Delta t}{\Delta x}\frac{\rho_{i,N_i-1}^{c}}{r_{i,N_i-1}} S_i^c(r_{i,N_i})
\end{aligned}$$

Setting

$$\phi(\rho^c) := \rho^c + \frac{\Delta t}{\Delta x}\frac{\rho_{i,N_i-1}^{c}}{r_{i,N_i-1}} S_i^c(r),$$

we get $\phi(R_i^c) = R_i^c$ and

$$\frac{\mathrm{d}\phi}{\mathrm{d}\rho^c}(\rho) = 1 + \frac{\Delta t}{\Delta x}\frac{\rho_{i,N_i-1}^{c}}{r_{i,N_i-1}}\frac{\partial S_i^c(r)}{\partial \rho^c} \geq 1 - \frac{\Delta t}{\Delta x}\frac{\rho_{i,N_i-1}^{c}}{r_{i,N_i-1}}\left\|\frac{\mathrm{d}S^c}{\mathrm{d}r}\right\|_\infty \geq 1 - \frac{\Delta t}{\Delta x}\left\|\frac{\mathrm{d}S^c}{\mathrm{d}r}\right\|_\infty \geq 0$$

if $\Delta t\left\|\frac{\mathrm{d}Q^c}{\mathrm{d}r}\right\|_\infty \leq \Delta x$. Hence $\rho_{i,N_i}^{c,\nu+1} \leq \phi(\rho_{i,N_i}^c) \leq R_i^c$.
Finally,

$$\begin{aligned}
\sum_{c=1}^{M}\rho_{i,N_i}^{c,\nu+1} &= \sum_{c=1}^{M}\rho_{i,N_i}^{c} - \frac{\Delta t}{\Delta x}\sum_{c=1}^{M}\left[\hat{\gamma}_i^c - F_{i,N_i-\frac{1}{2}}^{c}\right] \\
&\leq \sum_{c=1}^{M}\rho_{i,N_i}^{c} + \frac{\Delta t}{\Delta x}\sum_{c=1}^{M} F_{i,N_i-\frac{1}{2}}^{c} \\
&\leq \sum_{c=1}^{M}\rho_{i,N_i}^{c} + \frac{\Delta t}{\Delta x}\sum_{c=1}^{M}\frac{\rho_{i,N_i-1}^{c}}{r_{i,N_i-1}} S_i^c(r_{i,N_i})
\end{aligned}$$

Setting

$$\phi(\boldsymbol{\rho}) := \sum_{c=1}^{M}\rho^c + \frac{\Delta t}{\Delta x}\sum_{c=1}^{M}\frac{\rho_{i,N_i-1}^{c}}{r_{i,N_i-1}} S_i^c(r),$$

we get $\phi(\boldsymbol{\rho}) = R_i$ if $\sum_{c=1}^{M} \rho^c = R_i$ and

$$\begin{aligned}
\frac{\partial \phi}{\partial \rho^d}(\boldsymbol{\rho}) &= 1 + \frac{\Delta t}{\Delta x} \sum_{c=1}^{M} \frac{\rho^c_{i,N_i-1}}{r_{i,N_i-1}} \frac{\partial S^c_i(r)}{\partial \rho^d} \\
&\geq 1 - \frac{\Delta t}{\Delta x} \sum_{c=1}^{M} \frac{\rho^c_{i,N_i-1}}{r_{i,N_i-1}} \left\| \frac{\mathrm{d}S^c_i}{\mathrm{d}r} \right\|_\infty \\
&\geq 1 - \frac{\Delta t}{\Delta x} \max_c \left\| \frac{\mathrm{d}S^c_i}{\mathrm{d}r} \right\|_\infty \sum_{c=1}^{M} \frac{\rho^c_{i,N_i-1}}{r_{i,N_i-1}}
\end{aligned}$$

If $\Delta t \max_c \left\| \frac{\mathrm{d}Q^c}{\mathrm{d}r} \right\|_\infty \leq \Delta x$, then $1 - \frac{\Delta t}{\Delta x} \max_c \left\| \frac{\mathrm{d}S^c}{\mathrm{d}r} \right\|_\infty \geq 0$ and hence $\phi(\boldsymbol{\rho}) \leq R_i$, where we used that $\sum_{c=1}^{M} \frac{\rho^c_{i,N_i-1}}{r_{i,N_i-1}} = 1$.
Similarly, we assume that at the first cell of any outgoing road $j \in \mathcal{J}$, $\rho^{c,\nu}_{j,1} \in [0, R^c_j]$ for $c = 1, \ldots, M$, and $\sum_{c=1}^{M} \rho^{c,\nu}_{j,1} \leq R_j$, we show that the same holds for $\rho^{c,\nu+1}_{j,1}$.
We have that $\rho^{c,\nu+1}_{j,1} = \rho^{c,\nu}_{j,1} - \frac{\Delta t}{\Delta x} \left[F^c_{j,\frac{1}{2}} - \hat{\gamma}^c_j \right]$.
For positivity, the proof is similar to Lemma 2.4:

$$\begin{aligned}
\rho^{c,\nu+1}_{j,1} &= \rho^c_{j,1} - \frac{\Delta t}{\Delta x} \left[F^c_{j,\frac{1}{2}} - \hat{\gamma}^c_j \right] \\
&\geq \rho^c_{j,1} - \frac{\Delta t}{\Delta x} F^c_{j,\frac{1}{2}} \\
&= \rho^c_{j,1} - \frac{\Delta t}{\Delta x} \frac{\rho^c_{j,1}}{r_{j,1}} \min\left\{ D^c_j(r_{j,1}), S^c_j(r_{j,2}) \right\} \\
&\geq \rho^c_{j,1} - \frac{\Delta t}{\Delta x} \frac{\rho^c_{j,1}}{r_{j,1}} D^c_j(r_{j,1}) \\
&= \rho^c_{j,1} - \frac{\Delta t}{\Delta x} \frac{\rho^c_{j,1}}{r_{j,1}} Q^c(\min\{r_{j,1}, r^c_{j,cr}\}) \\
&= \rho^c_{j,1} - \frac{\Delta t}{\Delta x} \frac{\rho^c_{j,1}}{r_{j,1}} \min\{r_{j,1}, r^c_{j,cr}\} v^c_j(\min\{r_{j,1}, r^c_{j,cr}\}) \\
&\geq \rho^c_{j,1} - \frac{\Delta t}{\Delta x} \frac{\rho^c_{j,1}}{r_{j,1}} r_{j,1} v^c_j(\min\{r_{j,1}, r^c_{j,cr}\}) \\
&= \rho^c_{j,1} \left(1 - \frac{\Delta t}{\Delta x} v^c_j(\min\{r_{j,1}, r^c_{j,cr}\}) \right) \geq 0
\end{aligned}$$

if $\Delta t \|v^c\|_\infty \leq \Delta x$.

To prove that $\rho_{j,1}^{c,\nu} \leq R_j^c$, we compute

$$\begin{aligned}
\rho_{j,1}^{c,\nu+1} &= \rho_{j,1}^c - \frac{\Delta t}{\Delta x}\left[F_{j,\frac{1}{2}}^c - \hat{\gamma}_j^c\right] \\
&\leq \rho_{j,1}^c + \frac{\Delta t}{\Delta x}\hat{\gamma}_j^c \\
&= \rho_{j,1}^c + \frac{\Delta t}{\Delta x}\sum_{i=1}^m a_{ji}^c \hat{\gamma}_i^c \\
&= \rho_{j,1}^c + \frac{\Delta t}{\Delta x}\sum_{i=1}^m a_{ji}^c \frac{\rho_{i,N_i}^c}{r_{i,N_i}}\bar{\gamma}_i^c \\
&\leq \rho_{j,1}^c + \frac{\Delta t}{\Delta x}\sum_{i=1}^m a_{ji}^c \bar{\gamma}_i^c \\
&= \rho_{j,1}^c + \frac{\Delta t}{\Delta x}\bar{\gamma}_j^c \\
&\leq \rho_{j,1}^c + \frac{\Delta t}{\Delta x}S_j^c(r_{j,1})
\end{aligned}$$

Setting

$$\phi(\rho^c) := \rho^c + \frac{\Delta t}{\Delta x}S_j^c(r),$$

we get $\phi(R_j^c) = R_j^c$ and

$$\begin{aligned}
\frac{\mathrm{d}\phi}{\mathrm{d}\rho^c}(\rho^c) &= 1 + \frac{\Delta t}{\Delta x}\frac{\partial S_j^c(r)}{\partial \rho} \\
&\geq 1 - \frac{\Delta t}{\Delta x}\left\|\frac{\mathrm{d}S_j^c}{\mathrm{d}r}\right\|_\infty \geq 0
\end{aligned}$$

if $\Delta t\left\|\frac{\mathrm{d}Q^c}{\mathrm{d}r}\right\|_\infty \leq \Delta x$. Hence $\phi(\rho_j^c) \leq R_c^j$.

Finally, as above,

$$\begin{aligned}
\sum_{c=1}^{M} \rho_{j,1}^{c,\nu+1} &= \sum_{c=1}^{M} \rho_{j,1}^{c} - \frac{\Delta t}{\Delta x} \sum_{c=1}^{M} \left[F_{j,\frac{1}{2}}^{c} - \hat{\gamma}_{j}^{c} \right] \\
&\leq \sum_{c=1}^{M} \rho_{j,1}^{c} + \frac{\Delta t}{\Delta x} \sum_{c=1}^{M} \hat{\gamma}_{j}^{c} \\
&\leq \sum_{c=1}^{M} \rho_{j,1}^{c} + \frac{\Delta t}{\Delta x} \sum_{c=1}^{M} \sum_{i=1}^{m} \frac{\rho_{i,N_i}^{c}}{r_{i,N_i}} a_{ji}^{c} \bar{\gamma}_{i}^{c} \\
&\leq \sum_{c=1}^{M} \rho_{j,1}^{c} + \frac{\Delta t}{\Delta x} \sum_{c=1}^{M} \max_{i} \frac{\rho_{i,N_i}^{c}}{r_{i,N_i}} \sum_{i=1}^{m} a_{ji}^{c} \bar{\gamma}_{i}^{c} \\
&\leq \sum_{c=1}^{M} \rho_{j,1}^{c} + \frac{\Delta t}{\Delta x} \sum_{c=1}^{M} \max_{i} \frac{\rho_{i,N_i}^{c}}{r_{i,N_i}} \bar{\gamma}_{j}^{c} \\
&\leq \sum_{c=1}^{M} \rho_{j,1}^{c} + \frac{\Delta t}{\Delta x} \sum_{c=1}^{M} \max_{i} \frac{\rho_{i,N_i}^{c}}{r_{i,N_i}} S_{j}^{c}(r_{j,1}).
\end{aligned}$$

Setting

$$\phi(\boldsymbol{\rho}) := \sum_{c=1}^{M} \rho^{c} + \frac{\Delta t}{\Delta x} \sum_{c=1}^{M} \max_{i} \frac{\rho_{i,N_i}^{c}}{r_{i,N_i}} S_{j}^{c}(r),$$

we get $\phi(\boldsymbol{\rho}) = R_j$ if $\sum_{c=1}^{M} \rho^{c} = R_j$ and

$$\begin{aligned}
\frac{\partial \phi}{\partial \rho^{d}}(\boldsymbol{\rho}) &= 1 + \frac{\Delta t}{\Delta x} \sum_{c=1}^{M} \max_{i} \frac{\rho_{i,N_i}^{c}}{r_{i,N_i}} \frac{\partial S_{j}^{c}(r)}{\partial \rho^{d}} \\
&\geq 1 - \frac{\Delta t}{\Delta x} \sum_{c=1}^{M} \max_{i} \frac{\rho_{i,N_i}^{c}}{r_{i,N_i}} \left\| \frac{\mathrm{d}S_{j}^{c}}{\mathrm{d}r} \right\|_{\infty} \\
&\geq 1 - \frac{\Delta t}{\Delta x} \max_{c} \left\| \frac{\mathrm{d}S_{j}^{c}}{\mathrm{d}r} \right\|_{\infty} \sum_{c=1}^{M} \max_{i} \frac{\rho_{i,N_i}^{c}}{r_{i,N_i}} \\
&\geq 1 - \frac{\Delta t}{\Delta x} M \max_{c} \left\| \frac{\mathrm{d}S_{j}^{c}}{\mathrm{d}r} \right\|_{\infty}
\end{aligned}$$

If $M \Delta t \max_c \left\| \frac{\mathrm{d}Q^c}{\mathrm{d}r} \right\|_{\infty} \leq \Delta x$, then $1 - \frac{\Delta t}{\Delta x} M \max_c \left\| \frac{\mathrm{d}S_j^c}{\mathrm{d}r} \right\|_{\infty} \geq 0$ and hence $\phi(\boldsymbol{\rho}) \leq R_j$. □

3.1.2. Solver for 1×1 *junctions.*

If $|\mathcal{I}| = |\mathcal{J}| = 1$, and we adapt (15) by setting:

$$\hat{\gamma}_{i}^{c} = \hat{\gamma}_{j}^{c} = \frac{\rho_{i,N_i}^{c}}{r_{i,N_i}} \min \left\{ D_{i}^{c}(r_{i,N_i}), S_{j}^{c}(r_{j,1}) \right\}, \qquad c = 1, \ldots, M.$$

3.1.3. Solver for $m \times 1$ (merge) junctions.

If $|\mathcal{I}| = m$ and $|\mathcal{J}| = 1$, a class specific priority vector $P^c = (p_i^c)_{i\in\mathcal{I}} \in \mathbb{R}^m$, $p_i^c \geq 0$, $\sum_{i\in\mathcal{I}} p_i^c = 1$ is required to identify a unique solution (Garavello and Piccoli 2006), so that $\hat{\gamma}_i^c = p_i^c\,\hat{\gamma}_j^c$ for $i \in \mathcal{I}$. The corresponding fluxes are given by:

$$\begin{aligned}
\hat{\gamma}_i^c &= \frac{\rho_{i,N_i}^c}{r_{i,N_i}} \min\left\{ D_i^c(r_{i,N_i}), \max\left\{ p_i^c S_j^c(r_{j,1}), S_j^c(r_{j,1}) - \sum_{k\in\mathcal{I}\setminus\{i\}} D_k^c(r_{k,N_k}) \right\} \right\}, \qquad (21)\\
\hat{\gamma}_j^c &= \sum_{i=1}^{m} \hat{\gamma}_i^c,
\end{aligned}$$

for $c = 1, \ldots, M$, see also (Goatin et al. 2016).

3.1.4. Solver for $1 \times m$ (diverge) junctions.

If $|\mathcal{I}| = 1$ and $|\mathcal{J}| = m$, let $A^c = \left(\alpha_j^c\right)_{j\in\mathcal{J}}^T$, be the class specific distribution matrix, where $\alpha_j^c \geq 0$, $\sum_{j\in\mathcal{J}} \alpha_j^c = 1$. For the FIFO (first-in first-out) version (Garavello and Piccoli 2006), the fluxes at the junction are computed as:

$$\hat{\gamma}_j^c = \alpha_j^c \hat{\gamma}_i^c, \quad j \in \mathcal{J}, \qquad (22)$$

where

$$\hat{\gamma}_i^c = \frac{\rho_{i,N_i}^c}{r_{i,N_i}} \min_{j\in\mathcal{J}} \left\{ D_i^c(r_{i,N_i}), \frac{S_j^c(r_{j,1})}{\alpha_j^c} \right\}, \qquad (23)$$

for $c = 1, \ldots, M$.
The non-FIFO fluxes (Goatin et al. 2016, Herty and Klar 2004, Lebacque and Khoshyaran 2002) are instead given by:

$$\begin{aligned}
\hat{\gamma}_j^c &= \frac{\rho_{i,N_i}^c}{r_{i,N_i}} \min\left\{ \alpha_j^c D_i^c(r_{i,N_i}), S_j^c(r_{j,1}) \right\},\\
\hat{\gamma}_i^c &= \sum_{j\in\mathcal{J}} \hat{\gamma}_j^c,
\end{aligned} \qquad (24)$$

for $c = 1, \ldots, M$.

Remark 1. For simple diverges ($1\times m$), the weaker CFL (18) is sufficient to guarantee the invariance of $\mathcal{S}$. Indeed, let us assume that at the first cell of an outgoing road $j \in \mathcal{J}$, $\sum_{c=1}^M \rho_{j,1}^{c,\nu} \leq R_j$, we show that the same holds for $\sum_{c=1}^M \rho_{j,1}^{c,\nu+1}$. We consider

first a diverge following the FIFO rule (22)-(23). On an outgoing road j,

$$\begin{aligned}\sum_{c=1}^{M}\rho_{j,1}^{c,\nu+1} &= \sum_{c=1}^{M}\rho_{j,1}^{c} - \frac{\Delta t}{\Delta x}\sum_{c=1}^{M}\left[F_{j,\frac{1}{2}}^{c} - \hat{\gamma}_{j}^{c}\right]\\ &\le \sum_{c=1}^{M}\rho_{j,1}^{c} + \frac{\Delta t}{\Delta x}\sum_{c=1}^{M}\hat{\gamma}_{j}^{c}\\ &\le \sum_{c=1}^{M}\rho_{j,1}^{c} + \frac{\Delta t}{\Delta x}\sum_{c=1}^{M}\alpha_{j}^{c}\hat{\gamma}_{i}^{c}\\ &\le \sum_{c=1}^{M}\rho_{j,1}^{c} + \frac{\Delta t}{\Delta x}\sum_{c=1}^{M}\alpha_{j}^{c}\frac{\rho_{i,N_i}^{c}}{r_{i,N_i}}\frac{S_{j}^{c}(r_{j,1})}{\alpha_{j}^{c}}\\ &= \sum_{c=1}^{M}\rho_{j,1}^{c} + \frac{\Delta t}{\Delta x}\sum_{c=1}^{M}\frac{\rho_{i,N_i}^{c}}{r_{i,N_i}}S_{j}^{c}(r_{j,1}),\end{aligned}$$

Setting

$$\phi(\boldsymbol{\rho}) := \sum_{c=1}^{M}\rho^{c} + \frac{\Delta t}{\Delta x}\sum_{c=1}^{M}\frac{\rho_{i,N_i}^{c}}{r_{i,N_i}}S_{j}^{c}(r),$$

we get $\phi(\boldsymbol{\rho}) = R_j$ if $\sum_{c=1}^{M}\rho^{c} = R_j$ and

$$\begin{aligned}\frac{\partial\phi}{\partial\rho^{d}}(\boldsymbol{\rho}) &= 1 + \frac{\Delta t}{\Delta x}\sum_{c=1}^{M}\frac{\rho_{i,N_i}^{c}}{r_{i,N_i}}\frac{\partial S_{j}^{c}(r)}{\partial\rho^{d}}\\ &\ge 1 - \frac{\Delta t}{\Delta x}\sum_{c=1}^{M}\frac{\rho_{i,N_i}^{c}}{r_{i,N_i}}\left\|\frac{\mathrm{d}S_{j}^{c}}{\mathrm{d}r}\right\|_{\infty}\\ &\ge 1 - \frac{\Delta t}{\Delta x}\max_{c}\left\|\frac{\mathrm{d}S_{j}^{c}}{\mathrm{d}r}\right\|_{\infty}\sum_{c=1}^{M}\frac{\rho_{i,N_i}^{c}}{r_{i,N_i}}\\ &\ge 1 - \frac{\Delta t}{\Delta x}\max_{c}\left\|\frac{\mathrm{d}S_{j}^{c}}{\mathrm{d}r}\right\|_{\infty}\end{aligned}$$

If $\Delta t\max_c\left\|\frac{\mathrm{d}Q^c}{\mathrm{d}r}\right\|_{\infty} \le \Delta x$, then $1 - \frac{\Delta t}{\Delta x}\max_c\left\|\frac{\mathrm{d}S_j^c}{\mathrm{d}r}\right\|_{\infty} \ge 0$ and hence $\phi(\boldsymbol{\rho}) \le R_j$. If the non-FIFO rule (24) holds, we get

$$\begin{aligned}\sum_{c=1}^{M}\rho_{j,1}^{c,\nu+1} &= \sum_{c=1}^{M}\rho_{j,1}^{c} - \frac{\Delta t}{\Delta x}\sum_{c=1}^{M}\left[F_{j,\frac{1}{2}}^{c} - \hat{\gamma}_{j}^{c}\right]\\ &\le \sum_{c=1}^{M}\rho_{j,1}^{c} + \frac{\Delta t}{\Delta x}\sum_{c=1}^{M}\hat{\gamma}_{j}^{c}\\ &\le \sum_{c=1}^{M}\rho_{j,1}^{c} + \frac{\Delta t}{\Delta x}\sum_{c=1}^{M}\frac{\rho_{i,N_i}^{c}}{r_{i,N_i}}S_{j}^{c}(r_{j,1})\end{aligned}$$

and we proceed as above.

3.2. Boundary conditions

Let $F_{in} = (F_{in}^1, \dots, F_{in}^M)^T$ and $F_{out} = (F_{out}^1, \dots, F_{out}^M)^T$ be respectively the inflow boundary conditions at an origin node and the outflow boundary condition at a destination node (where we assume $F_{in}^c, F_{out}^c \geq 0$ for all $c = 1, \dots, M$).

In order not to miss vehicle counting when congestion spills back to the incoming nodes of the network, we assume the presence of a buffer of length $l^c(t)$ at the beginning of each entrance road j, see e.g. (Goatin et al. 2016, Samaranayake et al. 2018). The length of the buffer must be updated at every time step in order to choose the correct demand function to calculate the effective inflow at the origin node.

From (15), (21), we can define

$$\hat{\gamma}_{in}^c = \min\left\{ D^c(l^c), \max\left\{ \frac{1}{M} S_j^c(r_{j,1}), S_j^c(r_{j,1}) - \sum_{g \neq c} D^g(l^g) \right\} \right\}, \tag{25}$$

mimicking the presence of M independent buffers, one for each vehicle class and having the same priority to enter the network, where

$$D^c(l^c) = \begin{cases} Q_j^c(r_{cr}^c) & \text{if } l^c > 0\,, \\ F_{in}^c & \text{if } l^c = 0\,, \end{cases}$$

is the class c buffer demand. To update the buffer length at every time step, we set

$$l^c(t + \Delta t) = \max\left\{ l^c(t) + \Delta t \left(F_{in}^c(t) - \hat{\gamma}_{in}^c(t) \right), 0 \right\}. \tag{26}$$

At destination nodes, the effective outflow is computed as

$$\hat{\gamma}_{out}^c = \min\left\{ \frac{\rho_J^c}{r_{i,N_i}} D_i^c(r_{i,N_i}), F_{out}^c \right\}. \tag{27}$$

Above, $r_{j,1}$ and r_{i,N_i} are the density values respectively in the first and last cell of the concerned roads.

4. Numerical Results

The following tests have the purpose of assessing the capability of our general model to adapt to different situations and to capture intricate interactions between various vehicle types, as well as to highlight the differences with the more classical approach used in Joumaa et al. (2023), where the assumption of equal maximal densities was used. To this aim, we measure the overall traffic performance using two metrics: the total travel time and the CO_2 emissions. We consider a mix of three classes of vehicles: light-duty vehicles (e.g. cars), heavy-duty vehicles (e.g. trucks) and two-wheelers (e.g. bicycles). Then, we select cars as the reference class and represent the other classes in terms of passenger-car equivalents (`pce`) based on their impact on traffic flow (see Shalini and Kumar (2014), Van Lint et al. (2008)). More precisely, `pce` indicates the

number of passenger cars a specific vehicle type counts in relation to its capacity. In this work, unlike Van Lint et al. (2008), we consider for simplicity speed independent pce values and we assume, without loss of generality, that a truck is equivalent to two passenger cars and that three bikes take the same capacity as one car. This aligns with the findings of Pajecki et al. (2019), which report pce values for large heavy vehicles typically ranging between 1.45 and 2.10, and Prasetijo (2007), where the pce values for bicycles are generally within the range of 0.3 to 0.5. The pce values are then $\texttt{pce}_{cars} = 1$, $\texttt{pce}_{trucks} = 2$ and $\texttt{pce}_{bikes} = 1/3$, so if we consider that the maximal densities of cars, trucks, and bikes are respectively 150 $veh/km/lane$, 75 $veh/km/lane$ and 450 $veh/km/lane$, then multiplying by the pce values, the maximal density becomes 150 $\texttt{pce}/km/lane$ for all classes. In this work, we consider also class-specific lane discipline (i.e. on a two-lane road, cars can travel on both lanes, while trucks must occupy only the rightmost (or leftmost) lane), and we assume bikes can creep through larger vehicles when they are stopped, as though they could occupy 2.5 lanes. In this case, the maximal densities are $R^{cars} = 300\ \texttt{pce}/km$ for cars, $R^{trucks} = 150\ \texttt{pce}/km$ for trucks and $R^{bikes} = 375\ \texttt{pce}/km$ for bikes.

Given a network of L roads and a set of entrance nodes $\mathcal{I}_{in}$, the Total Travel Time (TTT) of a class c, i.e. the space and time integral of the corresponding density is defined as:

$$\mathrm{TTT}(\rho^c) = \Delta t \Delta x \sum_{\nu=0}^{T_f} \sum_{\ell=1}^{L} \sum_{j=0}^{N_\ell} \frac{\rho_{\ell,j}^{c,\nu}}{\texttt{pce}_c} + \Delta t \sum_{\nu=0}^{T_f} \sum_{o \in \mathcal{I}_{in}} \frac{l_o^{c,\nu}}{\texttt{pce}_c}\,. \tag{28}$$

where N_ℓ is the number of cells in link $\ell = 1, \ldots, L$, and T_f the number of time steps needed to cover the simulation time horizon. The TTT for all vehicle classes can then be computed directly using the total density r recovered from the simulation:

$$\mathrm{TTT}(r) = \sum_{c=1}^{M} \mathrm{TTT}(\rho^c) = \Delta t \Delta x \sum_{\nu=0}^{T_f} \sum_{\ell=1}^{L} \sum_{j=0}^{N_\ell} \sum_{c=1}^{M} \frac{\rho_{\ell,j}^{c,\nu}}{\texttt{pce}_c} + \Delta t \sum_{\nu=0}^{T_f} \sum_{o \in \mathcal{I}_{in}} \sum_{c=1}^{M} \frac{l_o^{c,\nu}}{\texttt{pce}_c}\,. \tag{29}$$

The total CO_2 emission TE_{CO2} of a given class c, i.e. the space and time integral of the product of the grams of CO_2 emitted per meter (i.e. class-specific emission factor) and the class-specific density, is defined as:

$$\mathrm{TE}_{CO2}(\rho^c) = \Delta t \Delta x \sum_{\nu=0}^{T_f} \sum_{\ell=1}^{L} \sum_{j=0}^{N_\ell} \frac{\rho_{\ell,j}^{c,\nu}}{\texttt{pce}_c}\, e_c(v^c(r_{\ell,j}^{\nu})) + \Delta t \sum_{\nu=0}^{T_f} \sum_{o \in \mathcal{I}_{in}} \frac{l_o^{c,\nu}}{\texttt{pce}_c}\, e_c(0)\,, \tag{30}$$

since $v^c(R^c) = 0$. Above, e_c is the function that gives us the grams of CO_2 emitted per meter by class c depending on the class-specific average speed, it is a weighted sum of the emission factor calculated with Copert model (see Copert v5.6.1) per each type of considered vehicle (see Appendix A, Figures A1 and A2). The fleet composition can be found in the report CITEPA (see Appendix A, tables A1 and A2). Notice that we divide the density by the pce values since we need the real number of vehicles in each class when calculating the emissions.

4.1. Network description

In the following tests, we consider the same network studied in Joumaa et al. (2023), consisting of 13 two-lane roads and 6 junctions, forming a main road and two additional routes available as secondary itineraries.

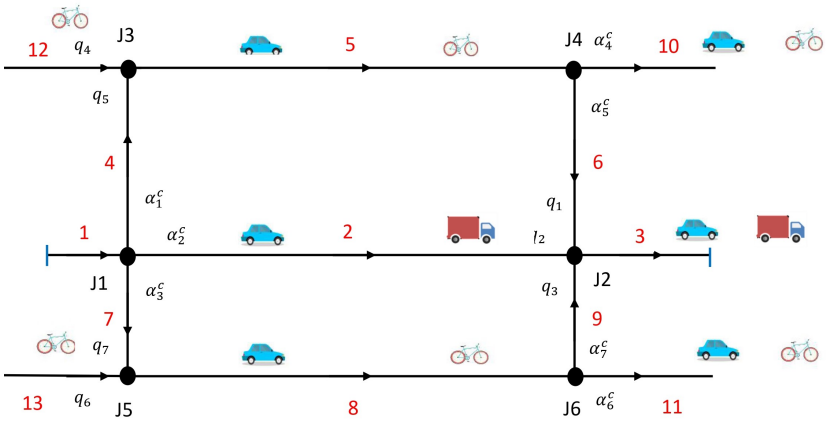

Figure 3.: Schematic representation of the network

Figure 3 is an illustration of the network, where we consider that cars enter only from road 1 and are allowed to circulate on the whole network with a speed of $V_{cars} = 70\ km/h$ on the main path (roads 1-2-3) and $V_{cars} = 50\ km/h$ on the secondary paths (roads 4-5-6, roads 7-8-9 and roads 10-11). Trucks, on the other hand, can only travel on the main path (roads 1-2-3) at a speed of $V_{trucks} = 50\ km/h$. Finally, bikes can only travel on roads 12-5-10 and 13-8-11 with a speed of $V_{bikes} = 20\ km/h$. Road 1 measures 0.1 km, roads 2, 5 and 8 have a length of 1 km, 0.3 km for roads 4 and 6 and finally 0.2 km for roads 3, 7, 9, 10, 11, 12 and 13. We consider a uniform grid with step size $\Delta x = 5\ m$ and the time is sampled with steps $\Delta t = 0.25\ s$. At the merge junction J2, we take $q_1 = q_3 = 0.3$ and consequently $q_2 = 0.4$ for all classes, meaning that vehicles coming from the main road have priority over those coming from the lateral ones. At the merge junctions J3 and J5, we give priority to the cars so the priority coefficients on roads 12 and 13 are $q_4 = q_6 = 0.1$. As for the distribution coefficients, we consider that cars do not have a preference at the diverge junctions J4 and J6, so we set $\alpha_4^{\text{cars}}, \alpha_5^{\text{cars}}, \alpha_6^{\text{cars}}, \alpha_7^{\text{cars}}$ equal to 0.5. For trucks, since they are only allowed on the main road, we set $\alpha_2^{\text{trucks}} = 1$ and 0 everywhere else, and finally we set $\alpha_4^{\text{bikes}} = \alpha_6^{\text{bikes}} = 1$ and 0 everywhere else, because bikes that enter from road 12 can only exit from road 10, and those that come from road 13 can only exit from road 11.

In the following, we present two different experiments, where we adopt the speed $v^c(r) = V^c(1 - \frac{r}{R^c})$ and we observe the variation of the cars' TTT and CO_2 emissions as a function of the distribution coefficient α at the diverge junction J1 and the percentage of cars and trucks θ_1 in the first experiment, and as a function of the percentage of cars and bikes θ_2 in the second experiment. Rerouting at J1 consists of gradually diverting cars from the primary route to the secondary paths. The idea is to improve the travel time for trucks by easing congestion on the main road. Nevertheless, rerouted vehicles will need to follow a longer path and share the lateral roads with bikes. To account for this, we allow the distribution coefficients of the cars at J1 to vary, i.e we set $\alpha_1^{\text{cars}} = \alpha_3^{\text{cars}} = \alpha \in [0, 0.5]$ towards the lateral roads 4 and 7, which implies

$\alpha_2^{\text{cars}} = 1 - 2\alpha$ on road 2.

In both experiments, the inflow at the network origin nodes is nonzero only on the time interval $[0, T]$, ensuring that all vehicles can enter in free flow and it is set equal to 0 on $]T, T_f]$, where $T_f > T > 0$ are prescribed time horizons. We set the supply F^c_{out} at exit nodes of roads 3, 10 and 11 equal to 20% of the maximal supply to induce congestion in the network, as if a traffic light was regulating outgoing traffic.

4.2. Experiment 1 (Different lane discipline for trucks)

In this experiment, we show how the model can be used to illustrate two completely different scenarios. In the first scenario, trucks are confined to one of the two lanes of the main road (roads 1-2-3), with maximal densities set at $R_{cars} = 300$ pce$/km$ for cars and $R_{trucks} = 150$ pce$/km$ for trucks. In the second scenario, trucks can use both lanes of the main road, and we thus assume equal maximal densities for both classes, namely $R_{cars} = R_{trucks} = 300$ pce$/km$. We note that our model does not address lane changing. Instead, we focus on roads with varying numbers of lanes to study lane discipline. For modeling lane changing in a macroscopic context, lane-specific models with interfacing terms between adjacent lanes allow for greater flexibility, see e.g. (Pan et al. 2021)

The network is initially empty and the boundary conditions at the entry and exit roads are as described in Section 3.2. We vary the proportion between trucks and cars by a parameter $\theta_1 \in [0, 1]$, as we set a global inflow

$$F^{ct}_{in} = 1800 \; veh/h$$

and

$$F^{cars}_{in}(t) = \theta_1 F^{ct}_{in}, \quad F^{trucks}_{in}(t) = (1 - \theta_1) F^{ct}_{in}, \qquad \text{for } t \in [0, T]$$

at the origin node at the entrance of road 1. For simplicity of analysis, we focus only on the interaction between cars and trucks, therefore we take $F^{bikes}_{in} \equiv 0$. The inflow stops at $T = 500$ s and the TTT and CO_2 emissions are calculated for both scenarios on a time horizon T_f large enough for all the vehicles to leave the network.

In Figures 4 and 5, we display the space-time diagrams of the vehicles' densities (in pce) on roads 2 and 3 of the network at $T = 600$ s for the case of $\alpha = 0$ (i.e. there is no rerouting of cars at junction J1) and $\theta_1 = 0.8$ (cars represent 80% of the total vehicle population). We notice the remarkable difference between the densities of cars and trucks in the first and second scenarios: the congestion of trucks is naturally much higher in scenario one, where they are allowed to travel on only one lane, than in the second scenario, where they are allowed two lanes. We also notice that cars reach the end of the road before trucks do, since they are faster and the network is initially empty, hence the red and green horizontal lines that we notice for cars and trucks respectively in scenario 1. However, they are not congested in the first scenario as much as they are in scenario 2, because they are less disturbed by the trucks and can keep moving when trucks are fully stopped (i.e. when trucks reach their maximal density).

Figure 6 shows the TTT for the total population in each scenario. We remark that the TTT in scenario 1 is maximal when we have trucks only (i.e. for $\theta_1 = 0$), then it decreases but stays higher than the TTT of scenario 2 until θ_1 reaches approximately 0.6, where they cross and it keeps decreasing until it reaches its minimum at $\theta_1 = 0.7$,

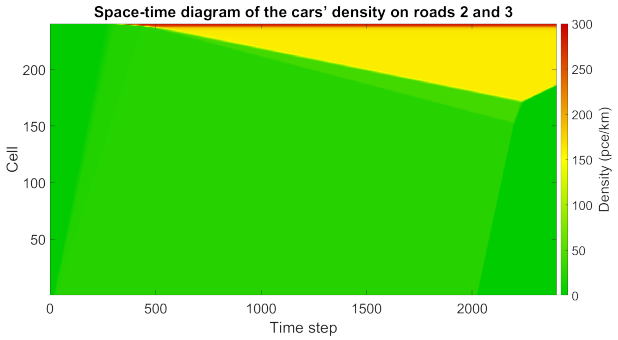

(a)

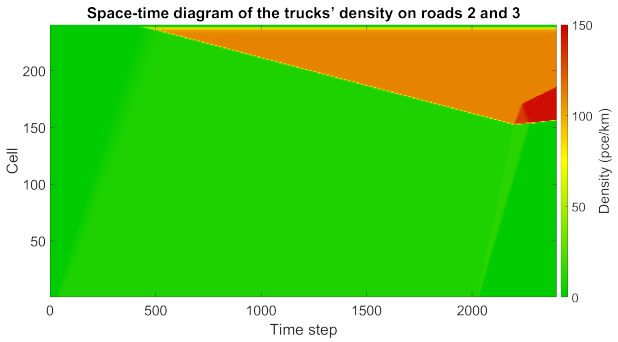

(b)

Figure 4.: Experiment 1 - Scenario 1: Trucks are allowed on one lane, cars and trucks have different maximal densities: $R_{cars} = 300$ pce$/km$, $R_{trucks} = 150$ pce$/km$, $T = 600$ s, $\alpha = 0$ and $\theta_1 = 0.8$.

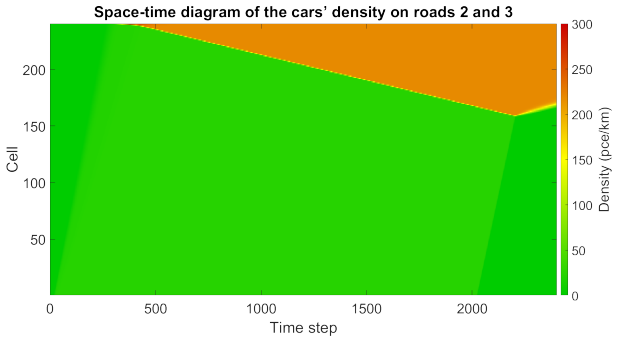

(a)

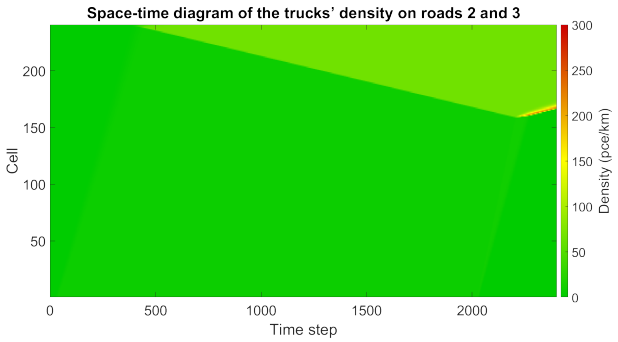

(b)

Figure 5.: Experiment 1 - Scenario 2: Trucks are allowed on two lanes, cars and trucks have equal maximal densities: $R_{cars} = R_{trucks} = 300$ pce$/km$, $T = 600$ s, $\alpha = 0$ and $\theta_1 = 0.8$.

then starts increasing again. This is due to the decrease in the number of trucks and the increase in the number of cars when θ_1 increases: since cars are faster, their TTT is smaller than the TTT of trucks (see Appendix B, Figures B1 and B3). However, when θ_1 becomes greater than 0.6, the TTT of the total population in the case where trucks are only allowed on one lane becomes lower than the TTT of the total population in the second case, which can be explained by the fact that cars can keep moving when trucks are completely stopped, so they can be faster and their TTT will decrease. We note that this was not the case when $\theta_1 \in [0, 0.6[$ because trucks are only allowed on one lane in the first case, while in the second case they are free to circulate on both lanes of the main road, which leads to a much lower TTT than in scenario 1. Moreover, the TTT of the total population, defined by the sum of the TTT of cars and trucks, is constant when $\theta_1 = 0$ and slightly decreases when α increases in both cases, when $\theta_1 \in]0, 0.6[$. The decrease w.r.t α becomes more significant when θ_1 becomes greater than or equal to 0.6 because the number of cars that are being rerouted is higher, so congestion is reduced on the exit road 3 and trucks move faster on the main road.
Figure 7 shows clearly that the CO_2 emissions of the total population are much higher in the first scenario compared to the second, since truck congestion is higher and their CO_2 emissions are dominant (much higher than the CO_2 emissions of the cars). The emissions decrease when α increases because the interaction between cars and trucks decreases with rerouting. The value of the emissions is constant for all values of α when $\theta_1 = 0$ in the case where trucks are allowed two lanes.

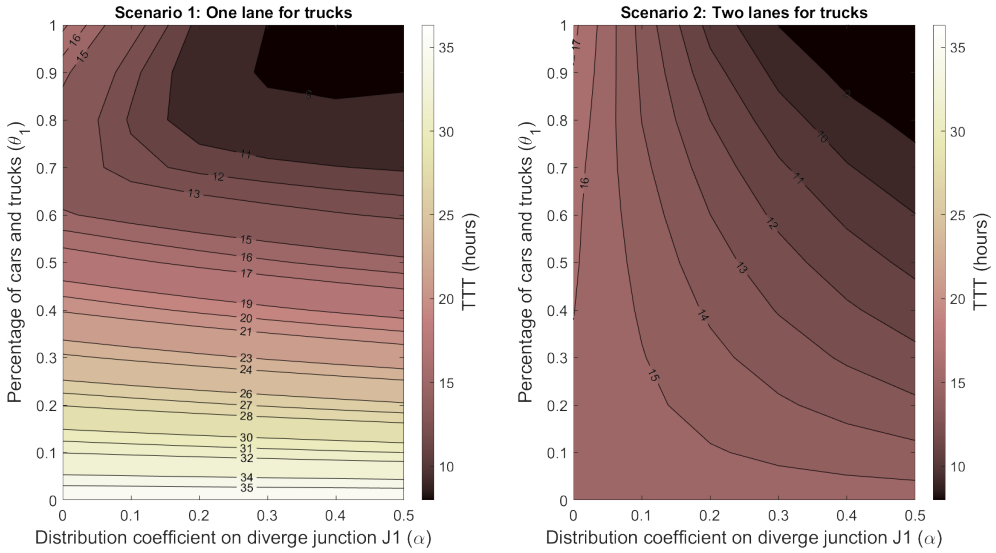

Figure 6.: Sum of the cars and trucks TTT (in hours) on the whole network as a function of the distribution coefficient $\alpha \in [0, 0.5]$ at the diverge junction J1 and the percentage of cars and trucks $\theta_1 \in [0, 1]$ for scenario 1 ($R_{cars} = 300$ pce$/km$, $R_{trucks} = 150$ pce$/km$) and scenario 2 ($R_{cars} = R_{trucks} = 300$ pce$/km$).

4.3. Experiment 2 (Modal shift)

The second experiment illustrates the effects of public policies encouraging the uptake of active transportation modes, by investigating the benefits of gradually shifting traffic flow from cars to bikes.
In this experiment, we consider three vehicle classes as presented in Figure 3, and we

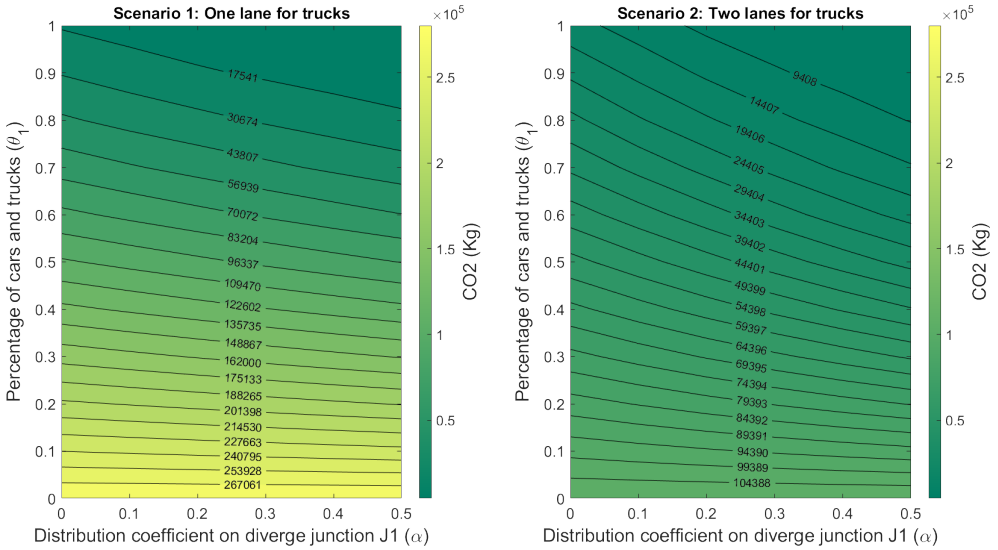

Figure 7.: Sum of the cars and trucks CO_2 emissions (in kilograms) on the whole network as a function of the distribution coefficient $\alpha \in [0, 0.5]$ at the diverge junction J1 and the percentage of cars and trucks $\theta_1 \in [0, 1]$ for scenario 1 ($R_{cars} = 300$ pce$/km$, $R_{trucks} = 150$ pce$/km$) and scenario 2 ($R_{cars} = R_{trucks} = 300$ pce$/km$).

compare two scenarios. More precisely, in the first case we allow bikes to share roads 5, 10, 8 and 11 with cars, whereas the second case models the presence of dedicated lanes for bikes, so that their presence does not impact car flow. To this aim, in the first case, we consider an initial density of 100 pce$/km$ for bikes on roads 12, 5, 10 and roads 13, 8, 11, the only roads where bikes can circulate. All other roads are initially empty. For the second case (with bikes on dedicated lanes), the network is initially empty. The maximal densities in both cases are $R_{cars} = 300$ pce$/km$, $R_{trucks} = 150$ pce$/km$, and $R_{bikes} = 375$ pce$/km$ for cars, trucks, and bikes respectively. The boundary conditions at the entry and exit roads are implemented as in Section 3.2. We set a global inflow

$$F_{in}^{cb} = 1800 \ veh/h,$$

and we consider that only 70% of the total motorized vehicle population are cars, and the rest are trucks. Moreover, in order to simulate a modal shift towards active modes of transport, we progressively shift 20% of cars to bikes by a parameter $\theta_2 \in [0, 1]$, setting:

$$F_{in}^{cars}(t) = (0.8\times0.7)F_{in}^{cb}+(1-\theta_2)(0.2\times0.7)F_{in}^{cb}, \quad F_{in}^{trucks}(t) = 0.3F_{in}^{cb} \qquad \text{for } t \in [0, T]$$

on road 1, and for the case without bike-dedicated lanes

$$F_{in}^{bikes}(t) = \texttt{pce}_{bikes} * \frac{\theta_2}{2}(0.2 \times 0.7)F_{in}^{cb}$$

on roads 12 and 13. The inflow stops at $T = 500$ s and the TTT and CO_2 emissions are calculated for T_f large enough for all the vehicles to leave the network.

Figures 8 and 9 show the space-time diagrams of the densities on roads 2, 3, 5, 10, 8 and 11 of the three populations at $T = 750$ s for the case where $\alpha = 0.5$ (all the cars are taking the lateral roads) and $\theta_2 = 0.5$. In the first scenario, we notice the high

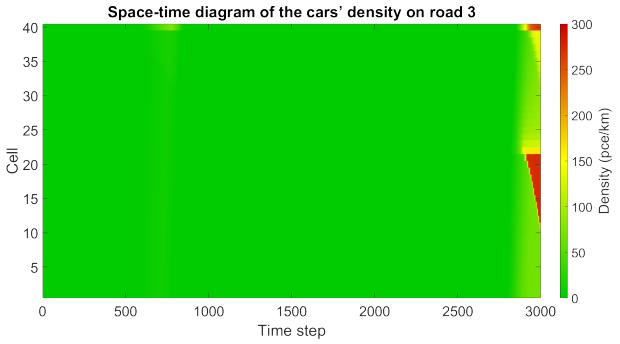

(a)

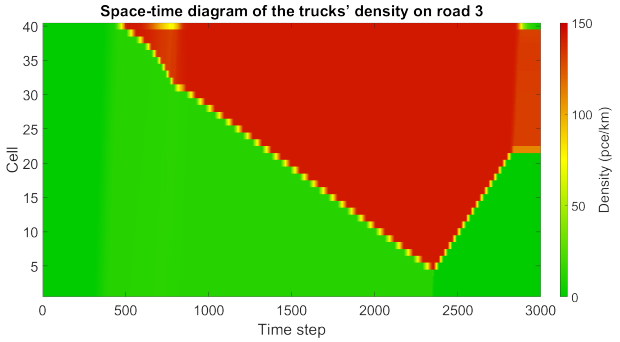

(b)

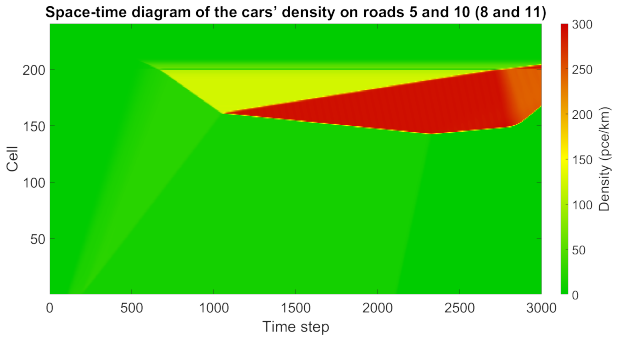

(c)

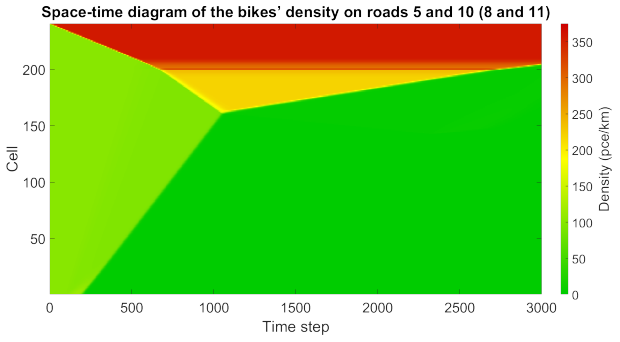

(d)

Figure 8.: Experiment 2 - Scenario 1: Bikes share the road with cars, $T = 750\ s$, $\alpha = 0.5$ and $\theta_2 = 0.5$.

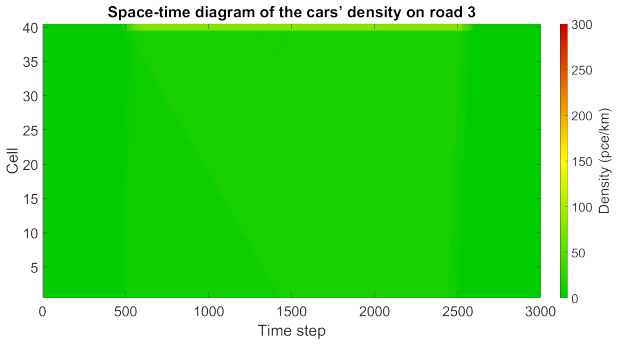

(a)

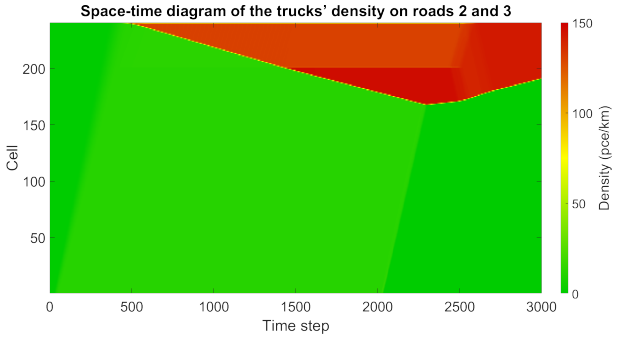

(b)

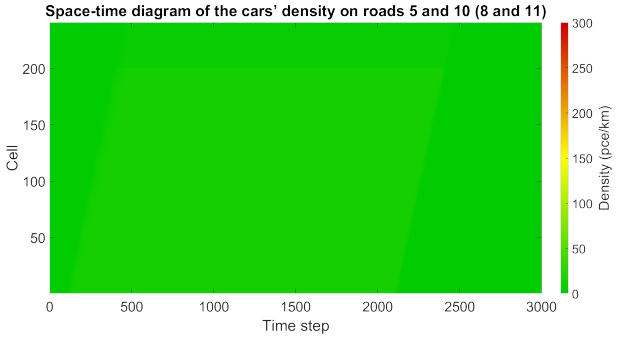

(c)

Figure 9.: Experiment 2 - Scenario 2: Bikes have their dedicated lane, $T = 750\ s$, $\alpha = 0.5$ and $\theta_2 = 0.5$.

level of congestion of bikes on roads 10 and 11 (cells 200 to 240), where they reach their maximal density. Moreover, we notice that even though cars are much faster than bikes, the latter reach the end of the roads before cars. This can be explained by the fact that bikes can creep between the cars when they are completely stopped. On roads 3, 5, 10, 8 and 11, we notice that cars are always in free flow since there are no interactions with bikes. This also explains the high level of truck congestion in scenario 2 on roads 2 and 3.

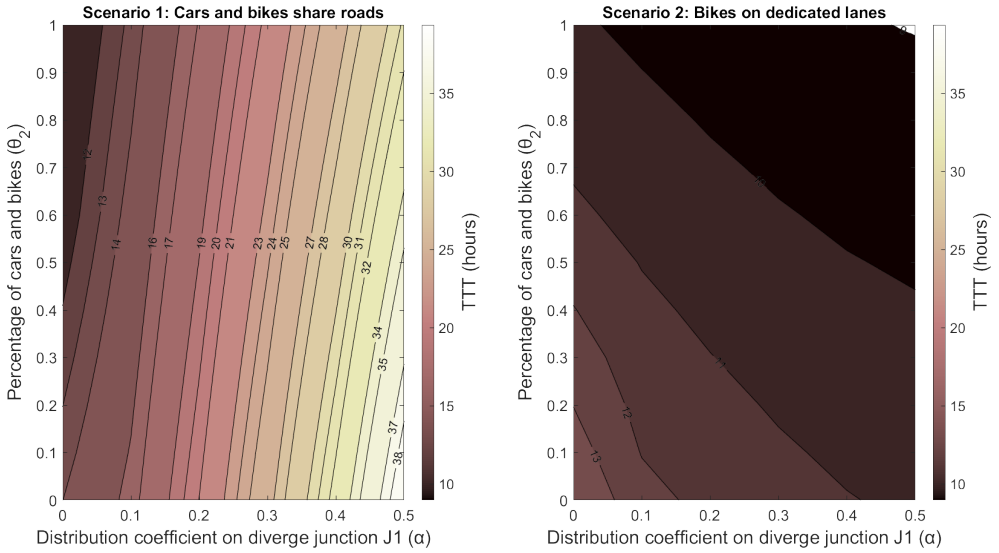

Figure 10.: Sum of the cars and trucks' TTT in hours on the whole network as a function of the distribution coefficient $\alpha \in [0, 0.5]$ at the diverge junction J1 and the percentage of cars and bikes $\theta_2 \in [0, 1]$ setting $R_{cars} = 300$ pce$/km$, $R_{trucks} = 150$ pce$/km$, and $R_{bikes} = 375$ pce$/km$, without bike dedicated lane (left) and with bike lane (right).

Figure 10 shows the significant difference between the TTT surface of cars and trucks in the two scenarios. The TTT is remarkably higher when bikes share roads with cars, due to congestion caused by bikes creeping on roads 5 and 8, which makes cars move more slowly. It also increases with α, since bikes are only present on the lateral roads. When bikes have dedicated lanes, the TTT does not depend much on alpha; however, the sum of the TTT of cars and trucks reaches its maximum point at $\alpha = 0$ and $\theta_2 = 0$, that is when there are only cars going straight on the main road, and decreases when θ_2 increases, i.e. when the number of cars decreases.
In Figure 11, we remark the significant decrease of the CO_2 emissions w.r.t. α in the second case. Moreover, the emissions of cars and trucks in the presence of bikes are much higher than in their absence. This reflects the fact that, with dedicated bike infrastructure, other vehicles can move faster, which decreases their CO_2 emissions, whereas in the presence of bikes sharing roads with cars, the latter experience slowdowns on roads 5 and 8. When α, i.e. the number of cars rerouted on lateral roads, increases, trucks can move faster on the main road in both cases. Nevertheless, when bikes are present, they impede cars, allowing trucks to exit from road 3 before cars arrive, avoiding slowdowns caused by car congestion. Moreover, we remark that the surface presenting the CO_2 emissions in the case where bikes share roads with cars has smaller variations, since cars' CO_2 emission increases significantly on roads 5 and 8 but on the contrary trucks' CO_2 emission decreases on roads 2 and 3. The separate

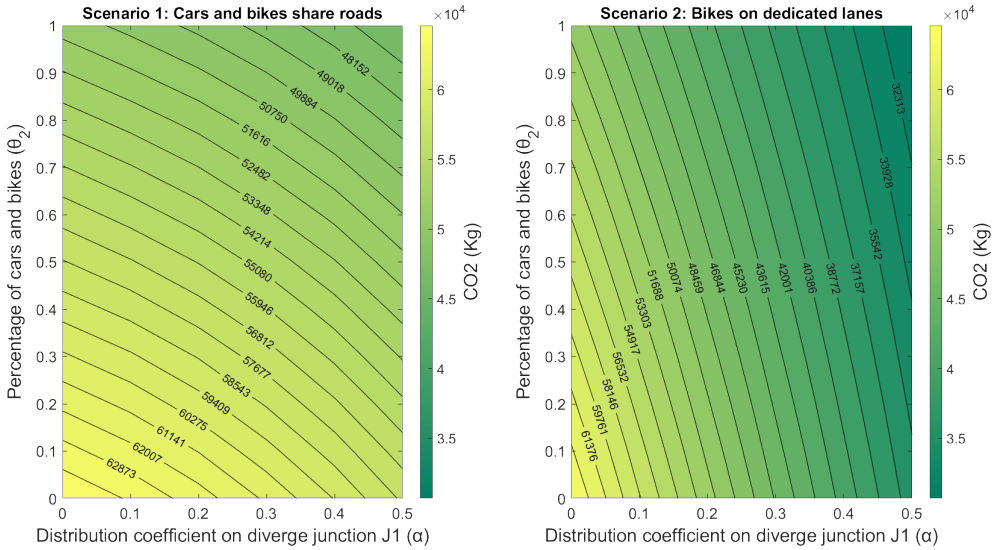

Figure 11.: Sum of the cars and trucks' CO_2 emissions (in kilograms) on the whole network as a function of the distribution coefficient $\alpha \in [0, 0.5]$ at the diverge junction J1 and the percentage of cars and bikes $\theta_2 \in [0, 1]$ setting $R_{cars} = 300$ pce$/km$, $R_{trucks} = 150$ pce$/km$, and $R_{bikes} = 375$ pce$/km$, without bike dedicated lane (left) and with bike lane (right).

surfaces for cars and trucks are shown in Appendix C, Figures C1 and C3 for the TTT and Figures C2 and C4 for the CO_2 emissions.

5. Conclusion

This study proposes a macroscopic model for heterogeneous traffic flow on general road networks that can deal with an arbitrary number of vehicle classes. The model considers general speed functions depending on the total density of vehicles and allows a fine tuning of the class-specific maximal densities to capture creeping phenomena and class-specific lane discipline. These properties are specifically relevant to describe shared road situations, as it typically occurs in urban environments. The extension to networks is based on a multi-class generalization of generic Riemann solvers at road junctions with an arbitrary number of incoming and outgoing links.
Using the "passenger-car-equivalent" notion, numerical experiments were performed, revealing that the model is able to deal with the complexities of traffic scenarios from real life. We computed the total travel time and the total emissions of CO_2 in a sample network, and showed how they can be influenced by different parameters, such as the distribution coefficient of cars (α) at diverge junctions and the rates of cars and trucks (θ_1) and cars and bikes (θ_2) entering the network. They differ when the composition of vehicle fleet varies, taking into account congested situations where cyclists can maneuver through a queue of cars and cars can pass beside a queue of trucks.

Future work in this area will include further evaluation of the multi-class macroscopic traffic flow model in more realistic and larger scale scenarios. This may ensure that the traffic flow behavior in real-world settings is accurately reflected by the model and it may also shed light on the variables that have higher influence on heterogeneous

traffic flow. Finally, the computational time of the proposed model is sufficiently low to allow for closed-loop optimization frameworks. This will help us understanding, for instance, the actions to be taken to reduce the negative effects of transportation on air quality within urban areas.

Acknowledgements

The authors are grateful to Eric Andoni for observations which greatly improved Proposition 2.4.

Disclosure statement

The authors report there are no competing interests to declare.

References

Muhammad Adnan. Passenger car equivalent factors in heterogenous traffic environment-are we using the right numbers? Procedia engineering, 77:106–113, 2014.

Sylvie Benzoni-Gavage and Rinaldo M Colombo. An-populations model for traffic flow. European Journal of Applied Mathematics, 14(5):587–612, 2003.

Maya Briani and Emiliano Cristiani. An easy-to-use algorithm for simulating traffic flow on networks: theoretical study. Netw. Heterog. Media, 9(3):519–552, 2014. ISSN 1556-1801. . URL https://doi.org/10.3934/nhm.2014.9.519.

R. Bürger, A. García, K. H. Karlsen, and J. D. Towers. A family of numerical schemes for kinematic flows with discontinuous flux. J. Engrg. Math., 60(3-4):387–425, 2008. ISSN 0022-0833. . URL https://doi.org/10.1007/s10665-007-9148-4.

Stéphane Chanut and Christine Buisson. Macroscopic model and its numerical solution for two-flow mixed traffic with different speeds and lengths. Transportation research record, 1852(1):209–219, 2003.

Felisia Angela Chiarello and Paola Goatin. Non-local multi-class traffic flow models. Networks and Heterogeneous Media, 14(2):371–387, 2019.

Giuseppe Maria Coclite, Mauro Garavello, and Benedetto Piccoli. Traffic flow on a road network. SIAM journal on mathematical analysis, 36(6):1862–1886, 2005.

R. Courant, K. Friedrichs, and H. Lewy. Über die partiellen Differenzengleichungen der mathematischen Physik. Math. Ann., 100(1):32–74, 1928. ISSN 0025-5831,1432-1807. . URL https://doi.org/10.1007/BF01448839.

Carlos F Daganzo. The cell transmission model, part II: network traffic. Transportation Research Part B: Methodological, 29(2):79–93, 1995.

Maria Laura Delle Monache, Paola Goatin, and Benedetto Piccoli. Priority-based riemann solver for traffic flow on networks. arXiv preprint arXiv:1606.07418, 2016.

Shimao Fan and Daniel B. Work. A heterogeneous multiclass traffic flow model with creeping. SIAM J. Appl. Math., 75(2):813–835, 2015. ISSN 0036-1399. . URL https://doi.org/10.1137/140977977.

Mauro Garavello and Benedetto Piccoli. Source-destination flow on a road network. 2005.

Mauro Garavello and Benedetto Piccoli. Traffic flow on networks, volume 1 of AIMS Series on Applied Mathematics. American Institute of Mathematical Sciences (AIMS), Springfield, MO, 2006. ISBN 978-1-60133-000-0; 1-60133-000-6. Conservation laws models.

Mauro Garavello, Ke Han, and Benedetto Piccoli. Models for vehicular traffic on networks, volume 9. American Institute of Mathematical Sciences Springfield, MO, USA, 2016.

Mauro Garavello et al. A review of conservation laws on networks. Networks Heterog. Media, 5(3):565–581, 2010.

Sosina Gashaw, Paola Goatin, and Jérôme Härri. Modeling and analysis of mixed flow of cars and powered two wheelers. Transportation research part C: emerging technologies, 89: 148–167, 2018.

Paola Goatin, Simone Göttlich, and Oliver Kolb. Speed limit and ramp meter control for traffic flow networks. Eng. Optim., 48(7):1121–1144, 2016. ISSN 0305-215X,1029-0273. . URL https://doi.org/10.1080/0305215X.2015.1097099.

S. K. Godunov. A difference method for numerical calculation of discontinuous solutions of the equations of hydrodynamics. Mat. Sb. (N.S.), 47 (89):271–306, 1959.

M. Herty, C. Kirchner, and S. Moutari. Multi-class traffic models on road networks. Commun. Math. Sci., 4(3):591–608, 2006. ISSN 1539-6746,1945-0796. URL http://projecteuclid.org/euclid.cms/1175797558.

Michael Herty and Axel Klar. Simplified dynamics and optimization of large scale traffic networks. Math. Models Methods Appl. Sci., 14(4):579–601, 2004. ISSN 0218-2025,1793-6314. . URL https://doi.org/10.1142/S0218202504003362.

Highway Capacity Manual. Transportation Research Board, National Research Council, Washington, DC, 1965.

Dongyao Jia, Kejie Lu, Jianping Wang, Xiang Zhang, and Xuemin Shen. A survey on platoon-based vehicular cyber-physical systems. IEEE communications surveys & tutorials, 18 (1):263–284, 2015.

Wen-Long Jin. A riemann solver for a system of hyperbolic conservation laws at a general road junction. Transportation Research Part B: Methodological, 98:21–41, 2017.

Agatha Joumaa, Paola Goatin, and Giovanni de Nunzio. A macroscopic model for multi-modal traffic flow in urban networks. In 26th IEEE International Conference on Intelligent Transportation Systems ITSC 2023, 2023.

JP Lebacque. The Godunov scheme and what it means for first order traffic flow models. In Proceedings of the 13th International Symposium on Transportation and Traffic Theory, Lyon, France, July, volume 2426. Citeseer, 1996.

JP Lebacque and MM Khoshyaran. First order macroscopic traffic flow models for networks in the context of dynamic assignment. In Transportation Planning: State of the Art, pages 119–140. Springer, 2002.

Michael W. Levin and Stephen D. Boyles. A multiclass cell transmission model for shared human and autonomous vehicle roads. Transportation Research Part C: Emerging Technologies, 62:103–116, 2016. ISSN 0968-090X. . URL https://www.sciencedirect.com/science/article/pii/S0968090X1500354X.

Jia Li, Di Chen, and Michael Zhang. Equilibrium modeling of mixed autonomy traffic flow based on game theory. Transportation research part B: methodological, 166:110–127, 2022.

Yanfeng Li and Jun Li. Multi-class dynamic network traffic flow propagation model with physical queues. Frontiers of Engineering Management, 4(4):399, 2017. . URL https://journal.hep.com.cn/fem/EN/abstract/article_20804.shtml.

M. J. Lighthill and G. B. Whitham. On kinematic waves. II. A theory of traffic flow on long crowded roads. Proc. Roy. Soc. London. Ser. A., 229:317–345, 1955. ISSN 0962-8444.

Haiyang Liu, Jian Wang, Kasun Wijayaratna, Vinayak V Dixit, and Steven Travis Waller. Integrating the bus vehicle class into the cell transmission model. IEEE Transactions on Intelligent Transportation Systems, 16(5):2620–2630, 2015.

S Logghe and Lambertus H Immers. Multi-class kinematic wave theory of traffic flow. Transportation Research Part B: Methodological, 42(6):523–541, 2008.

Rahul Nair, Hani S Mahmassani, and Elise Miller-Hooks. A porous flow approach to modeling heterogeneous traffic in disordered systems. Procedia-Social and Behavioral Sciences, 17: 611–627, 2011.

Robert Pajecki, Faisal Ahmed, Xiaobo Qu, Xinyi Zheng, Yanqun Yang, and Said Easa. Estimating passenger car equivalent of heavy vehicles at roundabout entry using micro-traffic simulation. Frontiers in Built Environment, 5:77, 2019.

Tianlu Pan, William H. K. Lam, Agachai Sumalee, and Renxin Zhong. Multiclass multilane model for freeway traffic mixed with connected automated vehicles and regular human-piloted vehicles. Transportmetrica A: Transport Science, 17(1):5–33, 2021. . URL https://doi.org/10.1080/23249935.2019.1573858.

Joewono Prasetijo. Capacity and traffic performance of unsignalized intersections under mixed traffic conditions. PhD thesis, Bochum, Univ., Diss., 2007, 2007.

Prema Somanathan Praveen and Venkatachalam Thamizh Arasan. Influence of traffic mix on pcu value of vehicles under heterogeneous traffic conditions. International Journal for Traffic & Transport Engineering, 3(3), 2013.

Zhen Sean Qian, Jia Li, Xiaopeng Li, Michael Zhang, and Haizhong Wang. Modeling heterogeneous traffic flow: A pragmatic approach. Transportation Research Part B: Methodological, 99:183–204, 2017.

Paul I Richards. Shock waves on the highway. Operations research, 4(1):42–51, 1956.

Samitha Samaranayake, Walid Krichene, Jack Reilly, Maria Laura Delle Monache, Paola Goatin, and Alexandre Bayen. Discrete-time system optimal dynamic traffic assignment (so-dta) with partial control for physical queuing networks. Transportation Science, 52 (4):982–1001, 2018. .

Kanakabandi Shalini and Brind Kumar. Estimation of the passenger car equivalent: a review. International Journal of Emerging Technology and Advanced Engineering, 4(6):97–102, 2014.

Kamonthep Tiaprasert, Yunlong Zhang, Chaodit Aswakul, Jian Jiao, and Xin Ye. Closed-form multiclass cell transmission model enhanced with overtaking, lane-changing, and first-in first-out properties. Transportation Research Part C: Emerging Technologies, 85:86–110, 2017.

Kamonthep Tuerprasert and Chaodit Aswakul. Multiclass cell transmission model for heterogeneous mobility in general topology of road network. Journal of Intelligent Transportation Systems, 14(2):68–82, 2010. . URL https://doi.org/10.1080/15472451003719715.

JWC Van Lint, Serge P Hoogendoorn, and Marco Schreuder. Fastlane: New multiclass first-order traffic flow model. Transportation Research Record, 2088(1):177–187, 2008.

Marie-Jette Wierbos, VL Knoop, FS Hänseler, and SP Hoogendoorn. A macroscopic flow model for mixed bicycle–car traffic. Transportmetrica A: transport science, 17(3):340–355, 2021.

G.C.K Wong and S.C Wong. A multi-class traffic flow model – an extension of lwr model with heterogeneous drivers. Transportation Research Part A: Policy and Practice, 36(9): 827–841, 2002. ISSN 0965-8564. . URL https://www.sciencedirect.com/science/article/pii/S0965856401000428.

HM Zhang and WL Jin. Kinematic wave traffic flow model for mixed traffic. Transportation Research Record, 1802(1):197–204, 2002.

Mengping Zhang, Chi-Wang Shu, George CK Wong, and SC Wong. A weighted essentially non-oscillatory numerical scheme for a multi-class lighthill–whitham–richards traffic flow model. Journal of Computational Physics, 191(2):639–659, 2003.

Peng Zhang, Ru-Xun Liu, S. C. Wong, and Shi-Qiang Dai. Hyperbolicity and kinematic waves of a class of multi-population partial differential equations. European J. Appl. Math., 17(2):171–200, 2006. ISSN 0956-7925. . URL https://doi.org/10.1017/S095679250500642X.

Appendix A. CO_2 Emissions, Copert model and CITEPA report

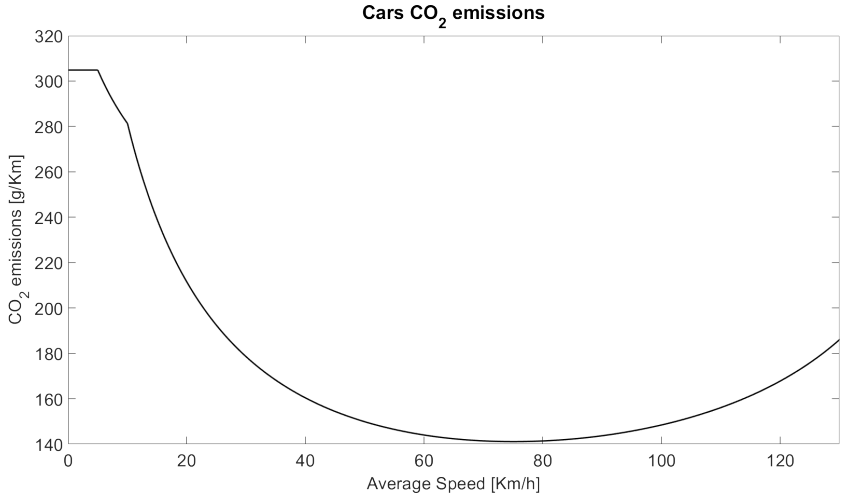

Figure A1.: CO_2 emissions of cars in g/Km as function of their average speeds.

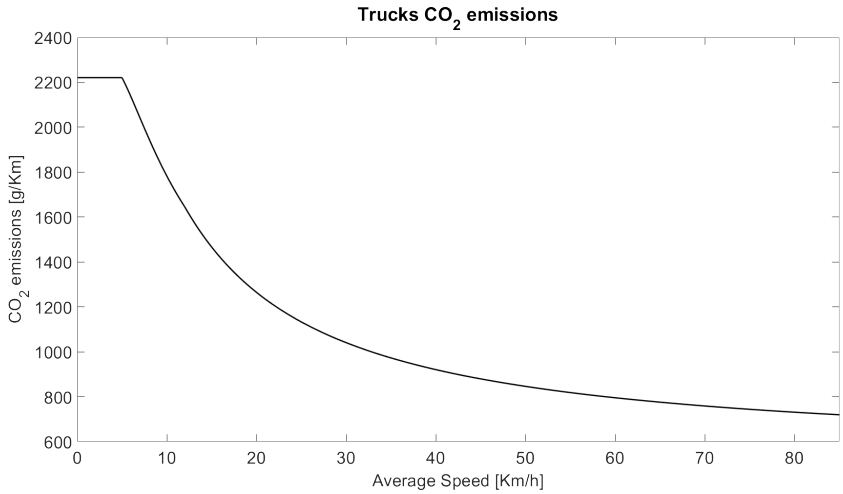

Figure A2.: CO_2 emissions of trucks in g/Km as function of their average speeds.

Appendix B. Experiment 1 - Separate plots for TTT and CO_2 of cars and trucks

Figure B1 clearly shows that the cars TTT in scenario 2 is higher than their TTT in scenario 1 for all values of α and θ_1. The two surfaces coincide only for $\theta_1 = 0$, that is when there are no cars. However, the difference between the two surfaces is the highest when $\alpha = 0$, then it decreases as α increases (i.e. the percentage of cars taking the secondary paths), since there is no overtaking on the lateral roads. We remark that the TTT in both models increases when θ_1 increases and reaches its maximum for $\theta_1 = 1$ and $\alpha = 0$, that is when we have only cars going on the main road.
Figure B2 shows the results for the car CO_2 emissions, which are consistent with the

Fuel/Energy Type	Euro 1	Euro 2	Euro 3	Euro 4	Euro 5	Euro 6 a/b/c	Euro 6 d-temp	Euro 6 d	-
Diesel	0.4	1	3.5	18.8	22.2	15.1	3.5	2.8	-
Petrol	0.2	0.5	0.9	3.6	6.2	12.4	4.2	3.1	-
LPG Bifuel $\sim$ Petrol	-	-	-	0.1	0.1	0.3	0.1	0.1	-
Electric	-	-	-	-	-	-	-	-	0.9

Table A1.: Fleet Composition Data for Cars (in %)

Fuel Type	Euro 2	Euro 3	Euro 4	Euro 5	Euro 6 d/e
Diesel	0.2	3.9	8.3	19.1	68.5

Table A2.: Fleet Composition Data for Trucks (in %)

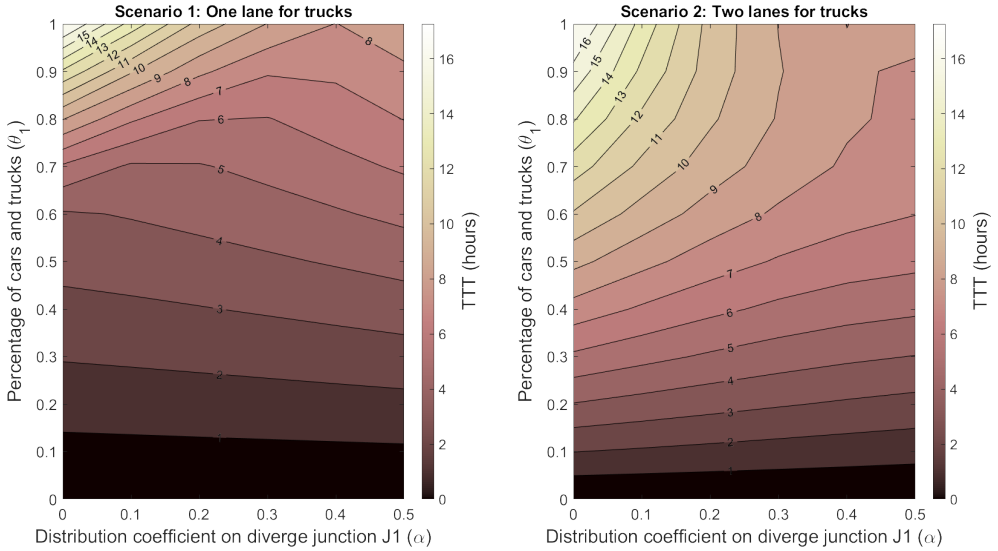

Figure B1.: Cars' TTT (in hours) on the whole network as a function of the distribution coefficient $\alpha \in [0, 0.5]$ at the diverge junction J1 and the percentage of cars and trucks $\theta_1 \in [0, 1]$ for scenario 1 ($R_{cars} = 300$ pce$/km$, $R_{trucks} = 150$ pce$/km$) and scenario 2 ($R_{cars} = R_{trucks} = 300$ pce$/km$).

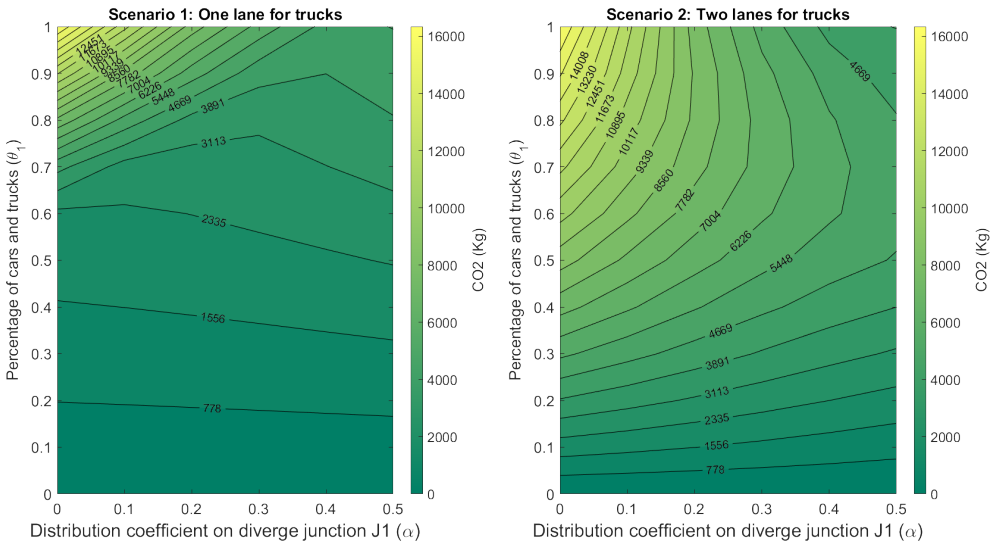

Figure B2.: Cars' CO_2 emissions (in kilograms) on the whole network as a function of the distribution coefficient $\alpha \in [0, 0.5]$ at the diverge junction J1 and the percentage of cars and trucks $\theta_1 \in [0, 1]$ for scenario 1 ($R_{cars} = 300$ pce$/km$, $R_{trucks} = 150$ pce$/km$) and scenario 2 ($R_{cars} = R_{trucks} = 300$ pce$/km$).

results of the TTT: the car CO_2 emissions in the second case are higher than in the first scenario, because they are slower when they cannot overtake queuing trucks and need longer time to leave the network. Similarly to the TTT, the difference between the two surfaces decreases as alpha increases. The CO_2 emissions of cars are the highest for $\theta_1 = 1$ and $\alpha = 0$.
In both figures, we remark that for $\theta_1 = 1$, the behavior is non-monotone: both TTT and CO_2 decrease until $\alpha = 0.4$, because the congestion on junction J2 decreases when α increases, but for $\alpha = 0.5$ they increase again, because all of cars take a longer path and thus travel for a longer distance.

The results showing the TTT and CO_2 emissions of trucks in Figures B3 and B4 are consistent. The TTT and CO_2 emissions of trucks in the case where they circulate on one lane are higher than their TTT when they are allowed two lanes. Moreover, both quantities decrease slightly when α increases, i.e. when cars are rerouted.

Appendix C. Experiment 2 - Separate plots for TTT and CO_2 of cars and trucks

Figure C1 shows the car TTT in the two cases (with and without bike dedicated lane). We can see that it is significantly higher in the case with bikes due to congestion caused by the presence of bikes on roads 5 and 8. It also increases when α increases, because bikes are only present on the lateral roads. The surface representing the case where bikes have their own lane is not very dependent on α; however, the cars' TTT reaches its maximum point at $\alpha = 0$ and $\theta_2 = 0$, that is when there are only cars going straight on the main road, and decreases when θ_2 increases, that is when we have less cars. In Figure C2, we see that the car CO_2 emissions for both cases obviously coincide for $\alpha = 0$, since it is the same situation for cars in both cases. For $\alpha = 0$, the surface with no bikes decreases when θ_2 increases, i.e. when the number of cars decreases, and

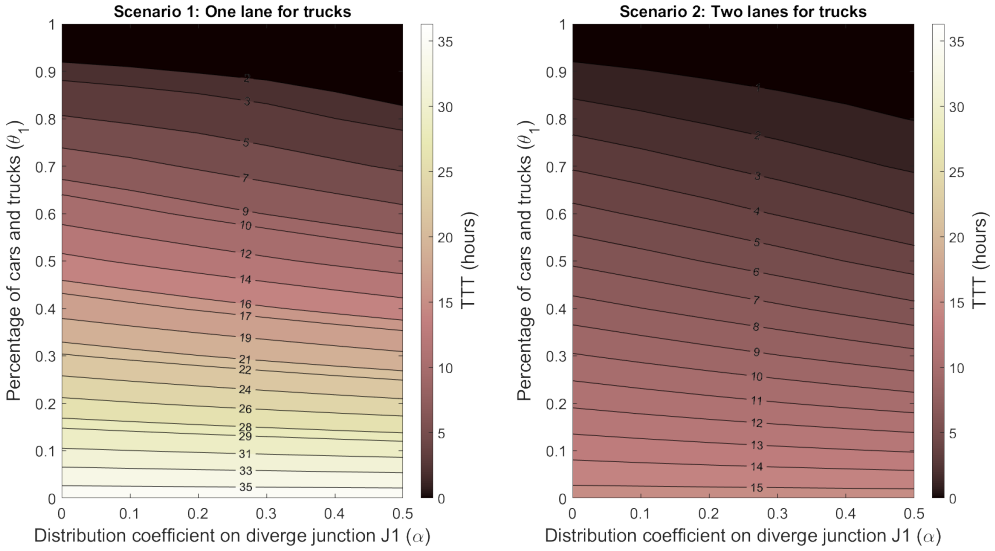

Figure B3.: Trucks' TTT (in hours) on the whole network as a function of the distribution coefficient $\alpha \in [0, 0.5]$ at the diverge junction J1 and the percentage of cars and trucks $\theta_1 \in [0, 1]$ for scenario 1 ($R_{cars} = 300$ pce$/km$, $R_{trucks} = 150$ pce$/km$) and scenario 2 ($R_{cars} = R_{trucks} = 300$ pce$/km$).

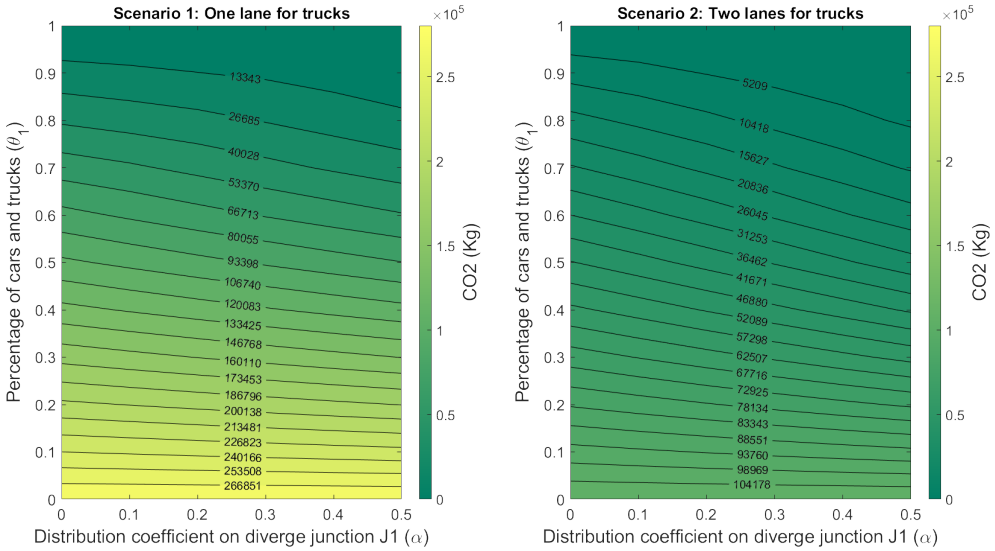

Figure B4.: Trucks' CO_2 emissions (in kilograms) on the whole network as a function of the distribution coefficient $\alpha \in [0, 0.5]$ at the diverge junction J1 and the percentage of cars and trucks $\theta_1 \in [0, 1]$ for scenario 1 ($R_{cars} = 300$ pce$/km$, $R_{trucks} = 150$ pce$/km$) and scenario 2 ($R_{cars} = R_{trucks} = 300$ pce$/km$).

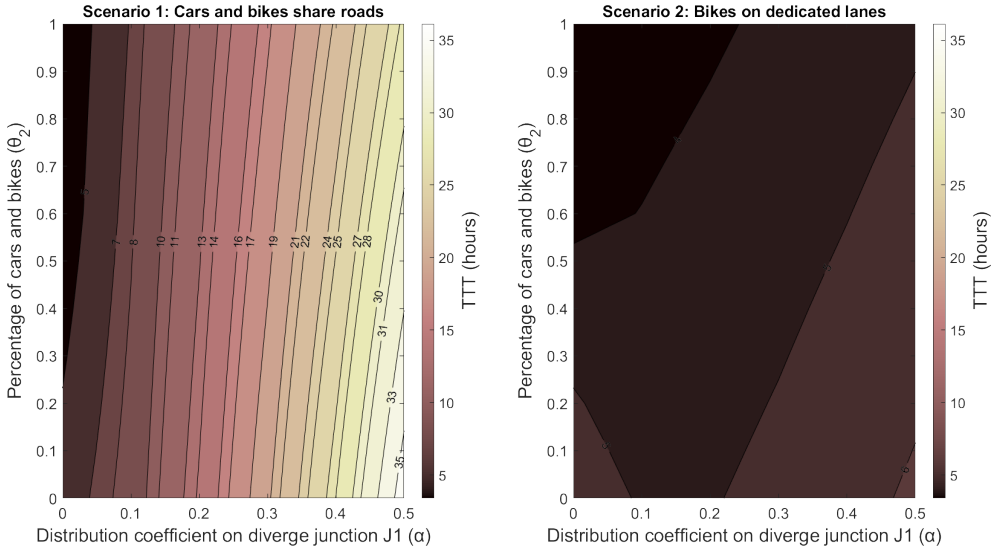

Figure C1.: Cars TTT (in hours) on the whole network as a function of the distribution coefficient $\alpha \in [0, 0.5]$ at the diverge junction J1 and the percentage of cars and trucks $\theta_1 \in [0, 1]$ setting $R_{cars} = 300$ pce$/km$, $R_{trucks} = 150$ pce$/km$, and $R_{bikes} = 375$ pce$/km$, without bike dedicated lane and with bike lane.

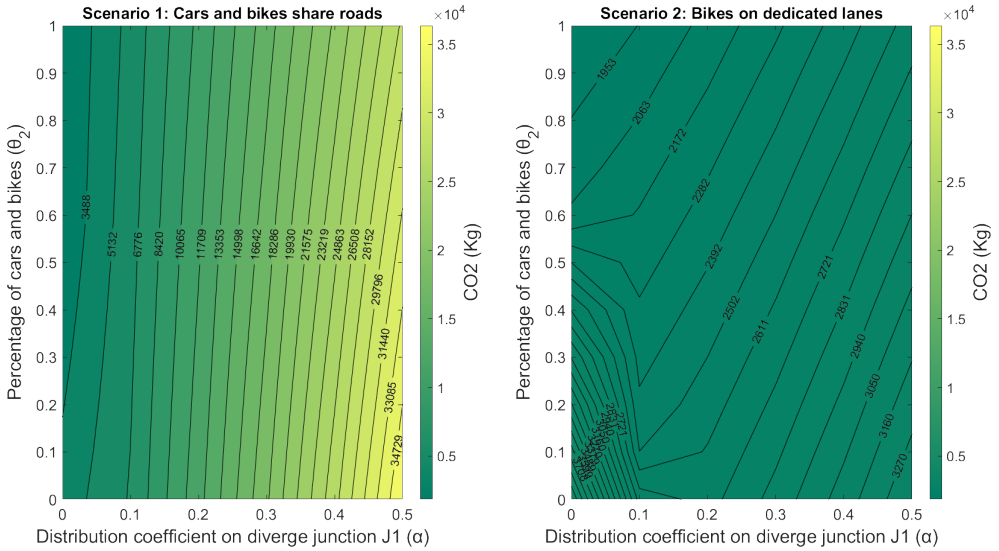

Figure C2.: Cars CO_2 emissions (in kilograms) on the whole network as a function of the distribution coefficient $\alpha \in [0, 0.5]$ at the diverge junction J1 and the percentage of cars and trucks $\theta_1 \in [0, 1]$ setting $R_{cars} = 300$ pce$/km$, $R_{trucks} = 150$ pce$/km$, and $R_{bikes} = 375$ pce$/km$, without bike dedicated lane and with bike lane.

does not vary much w.r.t other values of α. On the contrary, the surface with bikes increases significantly with α, due to the increase of congestion on roads 5, 10, 8 and 11.

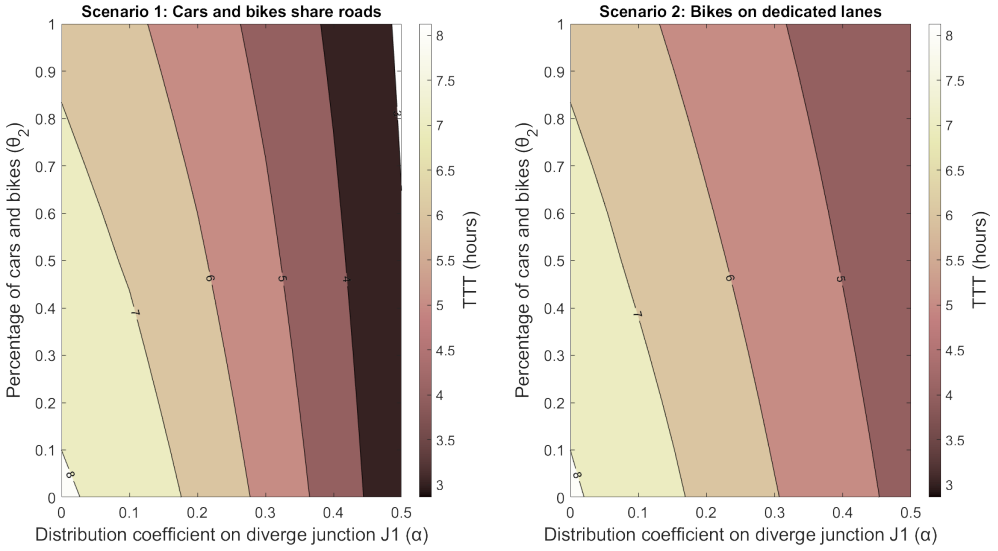

Figure C3.: Trucks' TTT (in hours) on the whole network as a function of the distribution coefficient $\alpha \in [0, 0.5]$ at the diverge junction J1 and the percentage of cars and trucks $\theta_1 \in [0, 1]$ setting $R_{cars} = 300$ pce$/km$, $R_{trucks} = 150$ pce$/km$, and $R_{bikes} = 375$ pce$/km$, without bike dedicated lane and with bike lane.

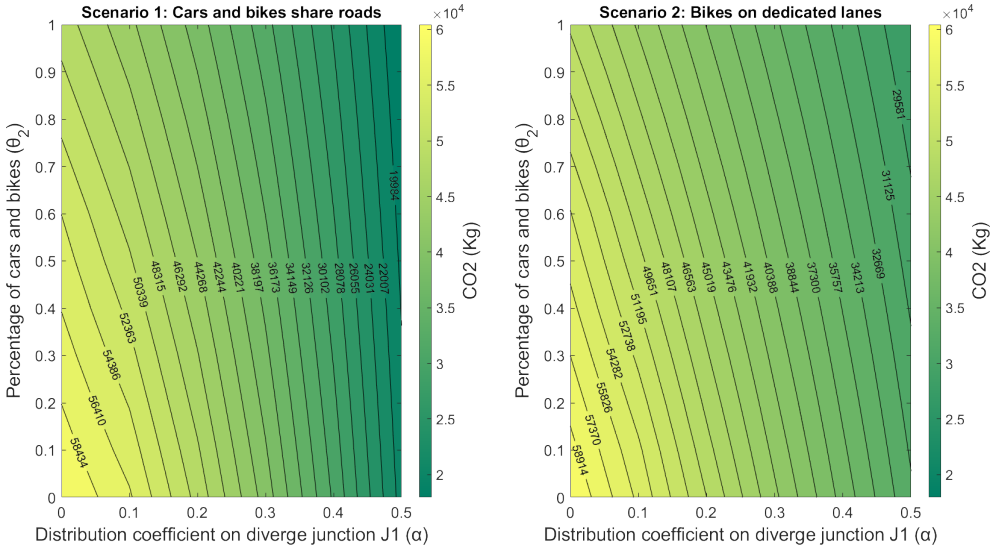

Figure C4.: Trucks' CO_2 emissions (in kilograms) on the whole network as a function of the distribution coefficient $\alpha \in [0, 0.5]$ at the diverge junction J1 and the percentage of cars and trucks $\theta_1 \in [0, 1]$ setting $R_{cars} = 300$ pce$/km$, $R_{trucks} = 150$ pce$/km$, and $R_{bikes} = 375$ pce$/km$, without bike dedicated lane and with bike lane.

Figures C3 and C4 show that, unlike for cars, the TTT and CO_2 emissions of trucks in the case without bikes are higher than in the case with bikes. This is easily explained by the fact that in the presence of bikes sharing lateral roads with cars, the latter take

more time to reach exit road 3, therefore trucks can leave faster before the arrival of the cars.